

1 **Measurement report: Enhanced photochemical formation of**
2 **formic and isocyanic acids in urban region aloft: insights**
3 **from tower-based online gradient measurements**

4 Qing Yang^{1,2}, Xiao-Bing Li^{1,2,*}, Bin Yuan^{1,2,*}, Xiaoxiao Zhang^{1,2}, Yibo Huangfu^{1,2}, Lei
5 Yang^{1,2}, Xianjun He^{1,2}, Jipeng Qi^{1,2}, Min Shao^{1,2}

6 ¹ Institute for Environmental and Climate Research, Jinan University, Guangzhou
7 511443, China

8 ² Guangdong-Hongkong-Macau Joint Laboratory of Collaborative Innovation for
9 Environmental Quality, Guangzhou 511443, China

10 * Corresponding authors: Xiao-Bing Li (lixiaobing@jnu.edu.cn), Bin Yuan
11 (byuan@jnu.edu.cn)

12 Abstract

13 Formic acid is the most abundant organic acid in the troposphere and has
14 significant environmental and climatic impacts. Isocyanic acid poses severe threats to
15 human health and could be formed through the degradation of formic acid. However,
16 the lack of vertical observation information has strongly limited the understanding of
17 their sources, particularly in urban regions with complex pollutant emissions. To
18 address this issue, we assessed the impact of long tubes on the measurement
19 uncertainties of formic and isocyanic acids and found that the tubing impact was
20 negligible. Then, we conducted continuous (27 days) vertical gradient measurements
21 (five heights between 5-320 m) of formic and isocyanic acids using long tubes based
22 on a tall tower in Beijing, China, during in the summer of 2021. ~~To address this issue,~~
23 ~~continuous (27 days) vertical gradient measurements (five heights between 5-320 m)~~
24 ~~of formic and isocyanic acids were made based on a tall tower in Beijing, China in~~
25 ~~summer of 2021.~~ Results show that the respective mean mixing ratios of formic and
26 isocyanic acids were 1.3 ± 1.3 ppbv and 0.28 ± 0.16 ppbv at 5 m and were 2.1 ± 1.9 ppbv
27 and 0.43 ± 0.21 ppbv at 320 m during the campaign. The mixing ratios of formic and
28 isocyanic acids were substantially enhanced in daytime and correlated with the diurnal
29 change of ozone. Upon sunrise, the mixing ratios of formic and isocyanic acids at
30 different heights simultaneously increased even in the residual layer. In addition,
31 positive vertical gradients were observed for formic and isocyanic acids throughout the
32 day. The positive vertical gradients of formic and isocyanic acids in daytime imply the
33 enhancement of their secondary formation in urban regions aloft, predominantly due to
34 the enhancements of oxygenated volatile organic compounds. Furthermore, the
35 afternoon peaks and positive vertical gradients of formic and isocyanic acids in
36 nighttime also indicate their minor contributions from primary emissions from ground-
37 level sources. ~~The afternoon peaks and positive vertical gradients of formic and~~
38 ~~isocyanic acids in nighttime indicate their dominant contributions from photochemical~~
39 ~~formations. Furthermore, the positive vertical gradients of formic and isocyanic acids~~

40 ~~in daytime imply the enhancement of their secondary formation in urban regions aloft,~~
41 ~~predominantly due to the enhancements of oxygenated volatile organic compounds.~~

42 The formation pathway of isocyanic acid through $\text{HCOOH-CH}_3\text{NO-HNCO}$ was
43 enhanced with height but only accounted for a tiny fraction of its ambient abundance.

44 The abundance and source contributions of formic and isocyanic acids in the
45 atmospheric boundary layer may be highly underestimated when being derived from
46 their ground-level measurements. With the aid of numerical modeling techniques,
47 future studies could further identify key precursors that drive the rapid formation of
48 formic and isocyanic acids, and quantitatively assess the impacts of the enhanced
49 formation of the two acids aloft on their budgets at ground level.

50 **1. Introduction**

51 Formic acid (HCOOH) is the simplest but the most abundant organic acid in the
52 troposphere. It has been widely measured in aqueous (clouds and aerosols) and gaseous
53 phases over urban, rural, and remote regions (*Kawamura and Kaplan, 1983; Chebbi
54 and Carlier, 1996; Kesselmeier et al., 1998; Yu, 2000*). As important contributors to the
55 acidity of precipitation, formic and acetic acids can account for 60% of the free acidity
56 in remote regions (*Galloway et al., 1982; Andreae et al., 1988*), and over 30% of the
57 free acidity in heavily polluted regions (*Keene and Galloway, 1984*). Formic acid is
58 also an important sink of hydroxyl radicals (OH) in clouds (*Jacob, 1986*), playing vital
59 roles in modulating the atmospheric aqueous-phase chemistry through changing pH-
60 dependent reaction rates of related constituents. An in-depth understanding of the
61 concentration levels, spatiotemporal variations, and sources of formic acid is key to
62 elucidating the formation mechanisms of atmospheric secondary pollution. However,
63 the sources and sinks of atmospheric formic acid are still poorly understood so far.

64 There have been many reported sources of atmospheric formic acid. Primary
65 emissions from vegetation activity (*Andreae et al., 1988; Kesselmeier et al., 1998*),
66 microbial metabolism (*Enders et al., 1992*), biomass burning (*Goode et al., 2000*), and
67 vehicle exhaust (*Kawamura et al., 2000*) were identified as important sources of formic
68 acid. Secondary formation from photochemical degradation of volatile organic
69 compounds (VOCs) is another significant source of formic acid (*Khare et al., 1999;
70 Veres et al., 2011; Le Breton et al., 2014; Liggio et al., 2017*). However, current
71 chemical transport models still highly underestimate ambient concentrations of formic
72 acid (*Stavrakou et al., 2011; Paulot et al., 2011; Millet et al., 2015*) and cannot well
73 reproduce its vertical variations. For example, Mattila et al. (2018) measured vertical
74 profiles of formic acid using an elevator on the Colorado Front Range BOA tower. They
75 found that formic acid mixing ratios generally decreased with height throughout the day,
76 but there were no known sources to explicitly explain the net surface emissions. [In
77 combination with vertical gradient and flux measurements of formic acid in a forest](#)

78 [ecosystem, Alwe et al. \(2019\) suggested that secondary formation, rather than primary](#)
79 [emission, is the major source of ambient formic acid.](#) The vertical distribution and
80 variation patterns of formic acid in the atmospheric boundary layer can provide
81 valuable information on the identification and determination of source contributions.
82 Nevertheless, the vertical variations and key drivers of formic acid, particularly in urban
83 regions, are still unclear due to the lack of adequate vertical observations.

84 Isocyanic acid (HNCO) is an inorganic acid and has attracted extensive concerns
85 worldwide in recent years due to its strong toxicity (*Wang et al., 2007; Jaisson et al.,*
86 *2011; Koeth et al., 2013*). Previous studies have reported that isocyanic acid is highly
87 soluble at physiological pH and the dissociated cyanate ions (NCO^-) are closely linked
88 to atherosclerosis, cataracts, and rheumatoid arthritis (*Mydel et al., 2010; Roberts et al.,*
89 *2011*). At present, there is no standard to clearly define the critical levels of isocyanic
90 acid pollution in ambient air (*Rosanka et al., 2020*). [The mixing ratio of HNCO in the](#)
91 [atmosphere exceeding 1 ppbv may endanger human health](#) (*Roberts et al., 2011*), [and](#)
92 [the protein carbamylation caused by HNCO in human body may induce various risks](#)
93 (*Verbrugge et al., 2015*). ~~A mixing ratio of 1 ppbv was considered the upper limit of~~
94 ~~ambient isocyanic acid, which is derived from the threshold of protein carbamylation~~
95 ~~reactions initiated by HNCO or NCO^- in human body~~ (*Verbrugge et al., 2015; Fulgham*
96 *et al., 2020*). Similar to formic acid, our understanding of isocyanic acid sources is also
97 very limited.

98 As reported in the literature, primary emissions of isocyanic acid are mainly from
99 combustion sources including cigarette smoke (*Hems et al., 2019*), gasoline and diesel
100 engine exhausts (*Wren et al., 2018*), and biomass combustion (*Wentzell et al., 2013; Li*
101 *et al., 2021; Chandra and Sinha, 2016*). Wet and dry deposition is known as the main
102 sink of isocyanic acid (*Roberts et al., 2014; Rosanka et al., 2020*). In addition, isocyanic
103 acid is highly soluble at atmospheric pH and can be hydrolyzed to NH_3 and CO_2 (*Zhao*
104 *et al., 2014; Roberts and Liu, 2019*). Secondary formation is another important source
105 of atmospheric isocyanic acid and the known precursors include amides (*Barnes et al.,*

106 2010), urea (Jathar et al., 2017), and nicotine (Roberts et al., 2011; Borduas et al.,
107 2016). Amides are reported to be the main precursors of isocyanic acid in urban regions
108 (Wang et al., 2020). Isocyanic acid is the oxidative degradation product of amides
109 initiated by OH radicals, NO₃, radicals, and Cl atoms (Barnes et al., 2010). In addition
110 to primary emissions from organic solvents and various industrial processes, amides
111 can be also formed through the atmospheric accretion reactions of organic acids with
112 amines or ammonia (Barnes et al., 2010; Yao et al., 2016). Vertical gradient
113 measurements of HNCO can help elucidate potential formation sources and
114 mechanisms.

115 ~~Amides are reported to be the main precursors of isocyanic acid in urban region~~
116 ~~(Wang et al., 2020). Isocyanic acid is the oxidative degradation product of amides~~
117 ~~initiated by OH radicals, NO₃, radicals, and Cl atoms (Barnes et al., 2010). In addition~~
118 ~~to primary emissions from organic solvents and various industrial processes, amides~~
119 ~~can be also formed through the atmospheric accretion reactions of organic acids with~~
120 ~~amines or ammonia (Barnes et al., 2010; Yao et al., 2016). The degradation of formic~~
121 ~~acid may be an important formation pathway of isocyanic acid in the atmosphere. For~~
122 ~~example, formamide could be formed from the atmospheric accretion reactions of~~
123 ~~formic acid with amines or ammonia and then produce isocyanic acid through reactions~~
124 ~~with OH radicals, NO₃, radicals, and Cl atoms. The vertical variations of formic acid~~
125 ~~will also have vital impacts on the sources and vertical distributions of isocyanic acid~~
126 ~~if the above-mentioned speculation is true. Unfortunately, the vertical distributions of~~
127 ~~isocyanic acid are also poorly understood due to the lack of measurements.~~

128 Chemical ionization mass ~~spectrometer~~spectrometry (CIMS) can effectively
129 detect and quantify atmospheric formic and isocyanic acids (Bannan et al., 2014;
130 Chandra and Sinha, 2016; Liggio et al., 2017; Mungall et al., 2018; Fulgham et al.,
131 2019). ~~However, the big mass, large volume, and strict operation environments of~~
132 ~~CIMS limit its wide application in making vertical measurements of formic and~~
133 ~~isocyanic acids.~~ CIMS has been widely used onboard aircraft or on towers to make

134 online vertical measurements of formic and isocyanic acids (*Liggio et al., 2017; Mattila*
135 *et al., 2018*). Aircraft can carry many types of instruments and achieve measurements
136 of a large suite of parameters (*Benish et al., 2020; Zhao et al., 2021*), but the cost is
137 also very expensive. Towers can provide vertical observations of target species by
138 setting up sites at different heights, building mobile platforms (elevators or baskets)
139 (*Mattila et al., 2018*), and drawing air from multiple heights to the ground-based
140 instruments through long tubes (*Hu et al., 2013; Yáñez-Serrano et al., 2018*). The usage
141 of long tubes is the most convenient and cost-effective method to make gradient
142 measurements of target gaseous species so far. However, interactions between gaseous
143 species and tubing walls may bring unexpected uncertainties for their measurements
144 (*Helmig et al., 2008a; Helmig et al., 2008b; Schnitzhofer et al., 2009; Karion et al.,*
145 *2010; Pagonis et al., 2017*). Therefore, the impacts of long tubing on measurements of
146 formic and isocyanic acids need to be elucidated.

147 In this study, we first assessed the effects of long perfluoroalkoxy-**alkane** (PFA)
148 Teflon tubes on measurements of formic and isocyanic acids. Vertical gradient
149 measurements of the two acids were made through long tubes on a tall tower in urban
150 Beijing, China. Then, the vertical variations and sources of the two acids were
151 investigated and discussed. At last, key conclusions and implications of this study were
152 summarized.

153 **2. Methods and materials**

154 **2.1. Site description and field campaign**

155 Vertical gradient measurements of gaseous species were made on the Beijing
156 Meteorological Tower, which is located on the campus of the Institute of Atmospheric
157 Physics (IAP), Chinese Academy of Sciences. Beijing is the capital city of China with
158 a population of over 20 million by 2020. Beijing has large anthropogenic emission
159 intensities and is suffering from severe air pollution problems (*Acton et al., 2020; Meng*
160 *et al., 2020; Tan et al., 2022*). The tower is located in the northern part of downtown

161 Beijing between the 3rd and 4th Ring Roads and is surrounded by urban roads,
162 expressways, residential areas, restaurants, urban landscaping, and parks. As a result,
163 concentrations of the primary pollutants at the tower site are mainly contributed by both
164 anthropogenic (e.g., vehicular exhausts, cooking, and household volatile chemical
165 products) and biogenic emissions. Detailed descriptions of the tower have been
166 provided in previous studies (*Acton et al., 2020; Yan et al., 2021*) and will not be
167 repeated here. The field campaign was carried out from July 17th to August 3rd, 2021.

168 **2.2. Instrumentation**

169 To obtain online gradient measurements of atmospheric trace gases, we
170 established a tower-based observation system using a combination of online
171 measurement techniques and long tubes [\(Figure S1\)](#). The system and related
172 assessments on the usage of long tubes have been explicitly described in our previous
173 study (*Li et al., 2023*) and will be briefly introduced here. [After removing fine particles](#)
174 [by PFA Teflon filters \(Whatman\) with a diameter of 46.2 mm and a pore size of 2 \$\mu\$ m,](#)
175 [ambient air at four altitudes on the tower \(namely 47, 102, 200, and 320 m\) was](#)
176 [simultaneously and continuously drawn to the ground through long PFA Teflon tubes](#)
177 [\(100, 150, 250, and 400 m; outer diameter: 1/2"; inner diameter: 0.374"\) by a vacuum](#)
178 [pump.](#)~~After removing fine particles by PFA Teflon filters, ambient air at four altitudes~~
179 ~~on the tower (namely 47, 102, 200, and 320 m) was simultaneously and continuously~~
180 ~~drawn to the ground through long PFA Teflon tubes (100, 150, 250, and 400 m; outer~~
181 ~~diameter: 1/2"; inner diameter: 0.374") by a pump.~~ The flow rate of the sample stream
182 in each tube was controlled by a critical orifice and ranged between ~~14~~[13-19-21](#)
183 standard liters per minute (SLPM), [as shown in table S1](#). The flow rates in long tubes
184 were retained as large as possible if instruments allowed to minimize the impact of gas-
185 surface interactions on measurements of targeted gaseous species (*Deming et al., 2019;*
186 *Li et al., 2023*). Two air-conditioned containers were placed next to each other on the
187 base of the tower and all the instruments were operated inside. An additional inlet of
188 the tube was mounted on the rooftop of the container (approximately 5 m above ground

189 level) to make measurements of trace gases near the surface. Therefore, the tower-based
190 observation system consisted of five inlet heights ranging from the ground level to 320
191 m. Inlets of the instruments were connected to the outlet of a Teflon solenoid valve
192 group, which was used to perform the switch of the inlet heights at time intervals of 4
193 minutes. Vertical gradient measurements of gaseous species were cyclically made over
194 periods of 20 minutes. Indoor PFA Teflon tubes were wrapped with insulation tubes and
195 were heated to prevent condensation of water and organic gases.

196 Formic and isocyanic acids were measured by a high-resolution time-of-flight
197 chemical ionization mass ~~spectrometer~~spectrometry with iodide reagent ion (ToF-
198 CIMS). Due to the high sensitivity to oxygenated volatile organic compounds (OVOCs),
199 the iodine ion source has been widely used in previous studies (Yuan et al., 2015;
200 Schobesberger et al., 2016; Mungall et al., 2018). A Filter Inlet for Gases and
201 AEROSols (FIGAERO) was used to perform the switch between the gas and particle
202 measurement modes (Lopez-Hilfiker et al., 2014). The ~~ionic~~ ion molecular reaction
203 (IMR) chamber is adjacent to the FIGAERO and utilizes a vacuum ultraviolet ion
204 source (VUV-IS). Iodide anion (I^-) is produced from the photoionization of methyl
205 iodide (CH_3I) in ~~MIR~~ IMR (Ji et al., 2020). During the measurements, I^- was produced
206 by introducing the CH_3I gas standard (1000 ppm, Dalian Special Gases, China) to the
207 IMR chamber at a flow rate of 2 standard cubic centimeters per minute (SCCM) in 200
208 SCCM high-purity nitrogen (N_2 , 99.9995%) by the VUV-IS. The pressure of the IMR
209 chamber was maintained at 70-80 mbar. ~~Due to the high sensitivity to oxygenated~~
210 ~~volatile organic compounds (OVOCs), the iodine ion source has been widely used in~~
211 ~~previous studies (Yuan et al., 2015; Schobesberger et al., 2016; Mungall et al., 2018).~~
212 Flow rates of the sample gas were maintained at 2 SLPM using a critical orifice. During
213 the field campaign, both gaseous and particle measurements were made through the
214 FIGAERO of the CIMS, but only gaseous measurements were analyzed in this study.
215 In a one-hour cycle, the first 24 min was allocated to make gaseous measurements
216 during which a complete vertical profile of a gaseous species can be obtained. In the

217 gaseous measurement mode, a rapid blank measurement was made for 10 s at 3-min
218 intervals in the first 21 min and a long-time blank measurement was made in the rest 3
219 min (Palm et al., 2019). During the first 21-min period of the one-hour cycle, another
220 inlet at 5 m was used to collect ambient particles using PTFE membrane filters
221 (Zefluor®, Pall Inc., USA). Therefore, the remaining 36 min of the one-hour cycle was
222 allocated to analyze the collected particle.~~During the field campaign, the FIGAERO~~
223 ~~was set to 24 minutes for gas measurements and 36 minutes for particle measurements~~
224 ~~in one-hour cycles. In gas mode, the first 21 minutes were used to measure ambient air~~
225 ~~and the last 3 minutes were used for instrument background measurements by~~
226 ~~introducing zero air at 3 SLPM. In addition, instrument background measurements were~~
227 ~~also made for 10 s at time intervals of 210 s (Palm et al., 2019).~~

228 Calibrations of the ToF-CIMS for formic and isocyanic acids were performed in
229 the laboratory before and after the field campaign. Standard solutions of formic acid
230 were evaporated using the liquid calibration unit (LCU, IONICON Analytik GmbH)
231 and then diluted to designated concentration gradients by being mixed with zero air at
232 five flow rates. The gas standard of isocyanic acid is unstable at ambient temperature
233 and thus no commercial gas cylinder was available. Instead, cyanuric acid solution was
234 put into a diffusion cell and heated to 300 °C to generate isocyanic acid gas at a stable
235 mixing ratio. An ion chromatograph was used to quantify the concentration of the gas
236 standard by measuring deionized water that absorbed the isocyanic acid gas. Detailed
237 information about the isocyanic acid calibration procedure has been provided in our
238 previous work (Wang et al., 2020). Impacts of the changes in ambient humidity on
239 measurements of the ToF-CIMS for both formic and isocyanic acids were determined
240 in the laboratory and were corrected ~~for eliminated~~ when calculating their respective
241 concentrations. Measured signals of the ToF-CIMS were processed using the Tofware
242 software package (version 3.0.3; Tofwerk AG, Switzerland).

243 A high-resolution proton-transfer-reaction quadrupole interface time-of-flight
244 mass spectrometry (PTR-ToF-MS) with both H₃O⁺ and NO⁺ ion chemistry was used to

245 [measure reported precursors of the two acids, such as isoprene, aromatics, OVOCs, and](#)
246 [amides.](#) ~~A high time resolution proton transfer reaction quadrupole interface time of~~
247 ~~flight mass spectrometer (PTR-ToF-MS) with both H₃O⁺ and NO⁺ ion chemistry was~~
248 ~~used to make some precursor measurements of the two acids, such as isoprene,~~
249 ~~aromatics, OVOCs, and amides.~~ Detailed information about the configuration and
250 operation setup of the PTR-ToF-MS has been provided in our previous studies (*Yuan et*
251 *al.*, 2017; *Wu et al.*, 2020; *Li et al.*, 2022). Mixing ratios of O₃, CO, and NO₂ were
252 measured by a UV absorption O₃ analyzer (T400, Teledyne API, USA), a gas filter
253 correlation CO analyzer (T300, Teledyne API, USA), and a trace level NO_x analyzer
254 (42i, Thermo, USA), respectively. Photolysis rates were measured by a PFS-100
255 photolysis spectrometer (Focused Photonics Inc.) on the rooftop of the container. The
256 planetary boundary layer height (PBLH) data was obtained from the website of the Air
257 Resources Laboratory (<https://ready.arl.noaa.gov/READYamet.php>). Measurements of
258 isocyanic acid and amides made in Guangzhou and Gucheng in China were also used
259 in this study for comparison, and more information about these observations can be
260 found in our previous papers (*Wang et al.*, 2020).

261 **2.3. Tubing assessment**

262 The tower-based observation system used long PFA Teflon tubes (hundreds of
263 meters in length) to draw air samples from different heights. The interactions between
264 tubing inner walls and organic compounds, namely the absorption/desorption of trace
265 gases, have nonnegligible impacts on their measurements after traversing such long
266 tubes (*Pagonis et al.*, 2017; *Deming et al.*, 2019). The equilibrium between the
267 absorption and desorption of organic compounds on tubing walls required distinct times,
268 namely tubing delay, for different species. For nonpolar/weak-polar organic compounds,
269 their tubing delays and measurement uncertainties after traversing long tubes are
270 dependent on their saturation concentrations and the flow rates of sample streams but
271 are independent of changes in humidity (*Krechmer et al.*, 2017; *Pagonis et al.*, 2017).
272 For some small polar organic compounds, their tubing delays and measurement

273 uncertainties after traversing long tubes are dependent on Henry's law coefficients and
274 are affected by changes in humidity (*Liu et al., 2019*). The performance of long PFA
275 Teflon tubes in measuring concentrations of nonpolar/weak-polar organic compounds
276 and inorganic species (e.g., ozone, NO, NO₂, and CO₂) has been assessed in our
277 previous work (*Li et al., 2023*). The impacts of long PFA Teflon tubes on measurements
278 of formic and isocyanic acids are still unclear and will be assessed in this study.

279 Long PFA Teflon tubes with an outer diameter of 1/2" and an inner diameter of
280 0.374" were used to draw air samples from different altitudes and thus were assessed.
281 At flow rates below 20 SLPM, suitable pressure drops can be maintained in these long
282 tubes for instrument operation (*Li et al., 2023*). The effects of long tubes on
283 measurements of formic and isocyanic acids were mainly assessed using the same
284 methods in the literature (*Li et al., 2023*). The tubing delay of formic acid is estimated
285 as the time required to reach 90% of the concentration change made at the tubing inlet.
286 The depassivation curve of formic acid measured at the air outlet end of the tubing was
287 used to calculate its tubing delay and was obtained by using a step-function change in
288 its concentration at the tubing inlet (*Pagonis et al., 2017; Deming et al., 2019*). The
289 formic acid signals were normalized to those measured at the beginning of the step-
290 function change and then were fitted using the double exponential method, as shown in
291 Figure 1. Finally, the tubing delay of formic acid was determined when the fitting line
292 decreased to 0.1. The previous study (*Li et al., 2023*) has reported that inorganic species
293 have small tubing delays even in a 400 m long tube. Therefore, tubing delays of
294 isocyanic acid in long tubes are not discussed in this study.

295 To further assess the impacts of long tubes (namely 100, 200, 300, and 400 m)
296 on measurements of formic and isocyanic acids in real environments, their ambient
297 mixing ratios measured through different lengths of tubes were intercompared by
298 running the inlets side by side at ground level. Ambient air samples were sequentially
299 drawn with and without the tubes through a Teflon solenoid valve group (Figure [S1S2](#)),
300 which was set to perform the switch at time intervals of 4 minutes. Instrument

301 backgrounds of the two species were measured for 10 s at time intervals of 1 minute by
302 passing zero air into the instrument at a flow rate of 3 SLPM. Inter-comparisons of the
303 formic acid and isocyanic acid measurements made through different lengths of tubes
304 were mainly performed using linear fittings ($y=kx+b$; k is the slope and b is the
305 intercept).

306 **3. Results and Discussions**

307 **3.1. Interactions between long tubes and the two acids**

308 As shown in Figure 1, signals of formic acid measured by the ToF-CIMS had a
309 tubing delay of 23 s after traversing the 400 m long tube at the flow rate of 13 SLPM.
310 In addition to the interactions between tubing walls and formic acid molecules (*Pagonis*
311 *et al.*, 2017; *Deming et al.*, 2019), molecular diffusion and dispersion (namely Taylor
312 dispersion) can cause the longitudinal mixing of gas molecules in the tubing and is also
313 an important factor contributing to the measured delays (*Karion et al.*, 2010). Molecular
314 diffusion and dispersion have strong dependences on molecular diffusion coefficients
315 and tubing flow rates (*Karion et al.*, 2010). The influential time of Taylor dispersion on
316 the measurements of formic acid through a 400 m long tube at the flow rate of 13 SLPM
317 was estimated to be only 2.9 s, which is much smaller than the measured tubing delay
318 (23 s) of formic acid. Therefore, the adsorption/desorption of formic acid molecules on
319 tubing inner walls plays a dominant role in determining the tubing delay.

320 For most organic compounds, the tubing delays generally depend on tubing flow
321 rates and their saturated concentrations (C^*) (*Li et al.*, 2023; *Deming et al.*, 2019). With
322 the increase in tubing length and flow rate, the tubing delays of organic compounds will
323 rapidly decrease (*Liu et al.*, 2019). Therefore, the tubing flow rates should be as large
324 as possible if the instrument could work normally. In addition, the tubing delays of
325 organic compounds generally increase with the decrease in their C^* (*Li et al.*, 2023). It
326 must be acknowledged that tubing delay is inevitable. The analysis time scales of
327 species concentrations measured through long tubes should be greater than their tubing

328 delays, especially for those with small C^* .

329 As shown in Figure S2S3(a), ambient mixing ratios of formic acid measured
330 through the 400 m long tube varied consistently with those measured without the tube
331 with mean values of 4.14 and 4.09 ppbv, respectively. The mixing ratios of formic acid
332 measured with the long tube were slightly higher in the daytime and lower at night in
333 comparison with those measured without the long tube. We also conducted a correlation
334 analysis between the mixing ratios of formic acid measured with and without long tubes.
335 As shown in Figure 2, the mixing ratios of formic acid measured with and without the
336 400 m long tube agreed within 20%, but the slope of the linear fitting ($k=0.84$) is lower
337 than 1. The differences of formic acid mixing ratios measured with and without the 400
338 m long tube were predominantly caused by the long-tail memory effect of the tubing
339 (Figure 1). For example, the mixing ratios of formic acid measured through the 400 m
340 long tube at night equaled to its ambient mixing ratios plus those released from the
341 tubing inner wall. The tubing delay of formic acid was determined when its mixing
342 ratios reached 90% of the change before entering the tubing. However, the long-tail
343 memory effect of the tubing mainly focused on the rest 10% of the change (Figure 1),
344 which required a much longer time to stabilize.

345 Impacts of the tubing memory effects will be accumulated due to the continuous
346 change in ambient concentrations of formic acid. To further assess the impacts of tubing
347 memory effects on measurement uncertainties of the two acids, differences between
348 mixing ratios of the species X (namely formic and isocyanic acids) measured with and
349 without long tubes at time t (denoted by $\delta[X]_t$) were calculated using Eq. (1):

$$350 \quad \delta[X]_t = [X_{without}]_t - [X_{with}]_t \quad (1)$$

351 where $[X_{with}]_t$ and $[X_{without}]_t$ refer to mixing ratios of the species X measured at
352 time t with and without long tubes, respectively; Δt is the change in time relative to
353 time t and was used to characterize the influential time of the memory effect. In addition,
354 the changes in mixing ratios of the species X measured using long tubes at time t relative
355 to its average mixing ratio over the previous time interval of Δt (denoted by $\Delta[X]_t$)

356 was also calculated using Eq. (2):

$$357 \quad \Delta[X]_t = [X_{with}]_t - \frac{\sum_{t-\Delta t}^t [X_{with}]}{\Delta t} \quad (2)$$

358 A strong correlation between $\delta[X]_t$ and $\Delta[X]_t$ could be captured at a certain Δt if
359 the tubing memory effect make essential contributions to measurement uncertainties of
360 the species X after traversing long tubes. For the 400 m long tubing, $\delta[X]_t$ and $\Delta[X]_t$
361 had the strongest correlation ($R^2=0.89$) when Δt was approximately 14 h (Figure
362 [S3S5](#)). As also shown in Figure 2(a), the mixing ratios of formic acid measured with
363 and without the 400 m long tube agreed well when $\Delta[HCOOH]$ approached to zero.
364 The decrease and increase in $\Delta[HCOOH]$ will enlarge measurement uncertainties of
365 formic acid using the long tube. In morning periods, ambient mixing ratios of formic
366 acid rapidly increased. As a result, the mixing ratios of formic acid measured through
367 the 400 m long tube were slightly lower than its ambient mixing ratios due to the
368 absorption of formic acid by tubing inner walls. In evening and nighttime periods, an
369 opposite phenomenon was observed due to the desorption of formic acid from tubing
370 inner walls (Figure [S2S3](#)). In addition to the 400 m long tube, impacts of the tubes with
371 lengths of 100, 200, and 300 m on measurements of formic acid were also assessed, as
372 shown in Figures 2(c) and 3(a). The usage of tubes with lengths of 100, 200, and 300
373 m has negligible impacts on the measurements of formic acid.

374 In contrast to formic acid, the usage of long tubes had minor impacts on the
375 measurements of isocyanic acid. The mixing ratios of isocyanic acid measured with and
376 without the 400 m long tube varied consistently ($k=0.86$, $R^2=0.90$) with mean values of
377 0.25 and 0.26 ppbv, respectively (Figure [S2S3](#)). As shown in Figure 2(b), $\Delta[HNCO]$
378 is evenly distributed on both sides of the 1:1 line. Therefore, the changes in ambient
379 concentrations of isocyanic acid do not have significant impacts on the measurements
380 of isocyanic acid through the long tubes. As also shown in Figure 3(b), $\delta[HNCO]$ and
381 $\Delta[HNCO]$ of isocyanic acid were independent of the changes in isocyanic acid mixing
382 ratios. The R^2 values of linear fittings were less than 0.21 for the isocyanic acid
383 measurements made using different lengths of tubes. This is consistent with the results

384 reported in the literature (*Helmig et al., 2008a; Helmig et al., 2008b; Li et al., 2023*)
385 that inorganic species with low reactivities can be well measured using long PFA Teflon
386 tubes. The test results confirm that the measurements of formic and isocyanic acids
387 made through long tubes can be used to characterize their vertical and temporal
388 variations.

389 **3.2. Vertical variations and sources of formic acid**

390 Time series of formic acid and ozone mixing ratios at 5 and 320 m are shown in
391 Figure 4. The concentrations of formic acid and ozone exhibited similar diurnal and
392 inter-diurnal variations at different altitudes during the campaign. Hourly mean mixing
393 ratios of ozone exhibited strong temporal variations with an average of 43.5 ± 25.3 ppbv
394 at 5 m and an average of 53.5 ± 25.0 ppbv at 320 m. Hourly mean mixing ratios of formic
395 acid at 5 m ranged between 0.1-6.6 ppbv with an average of 1.3 ± 1.3 ppbv at 5 m, which
396 is comparable to those observed in other megacities, such as Shenzhen (1.2 ppbv) in
397 China (*Zhu et al., 2019*), London (1.3 ppbv) in UK (*Bannan et al., 2017*), and Los
398 Angeles (2.0 ppbv) in USA (*Yuan et al., 2015*). By contrast, hourly mean mixing ratios
399 of formic acid at 320 m had an average of 2.1 ± 1.9 ppbv, approximately 1.6 times higher
400 than that at 5 m. The temporal variability of formic and isocyanic acids were mainly
401 caused by the diurnal and inter-diurnal changes in meteorological conditions (e.g., solar
402 radiation and PBLH).

403 Before July 12th, the daily maximum hourly mixing ratios of ozone at 5 m all
404 exceeded 100 ppbv, indicating the enhanced formation of secondary air pollutants
405 associated with photochemical reactions. The mixing ratios of formic acid measured
406 before July 12th were also prominently larger than those measured after, suggesting
407 important contributions from photochemical formations. [The photochemical formation](#)
408 [of secondary pollutants was weak from July 13th to 30th due to the cloudy and rainy](#)
409 [weather. Because of the precipitation, weak solar radiation \(characterized by small](#)
410 [j\(NO₂\) values\) and small PBLHs were observed from July 13th to 30th, largely](#)
411 [suppressing the photochemical formation of secondary air pollutants.](#) After August 1st,

412 low mixing ratios of ozone and formic acids were observed along with the occurrence
413 of favorable dilution conditions characterized by high PBLHs.

414 As shown in Figure 5, the mixing ratios of formic acid measured at the five
415 altitudes (namely 5, 47, 102, 200, and 320 m) exhibited similar diurnal patterns. After
416 sunrise (~6:00 LT), formic acid mixing ratios increased rapidly at each altitude before
417 reaching the peak between 14:00-16:00 LT and then continuously declined before
418 sunrise the following day. Similar diurnal variation patterns of formic acid were also
419 observed at other urban sites (*Veres et al., 2011*), rural sites (*Hu et al., 2022*), and remote
420 sites (*Schobesberger et al., 2016*). The diurnal variation patterns of formic acid were
421 highly similar to those of ozone (a typical secondary pollutant) but were different from
422 those of VOCs from primary emissions. Taking toluene as an example, toluene is a
423 typical VOC tracer of anthropogenic emission sources in urban regions, such as
424 industrial processes and vehicular exhausts (*Fang et al., 2016; Skorokhod et al., 2017*),
425 and is also an important precursor of ozone (*Yuan et al., 2012*). The mixing ratios of
426 toluene exhibited opposite diurnal variation patterns to those of ozone and formic acids
427 with the minima occurring at around 14:00 LT. The lower mixing ratios of toluene in
428 daytime than in nighttime were predominantly caused by the enhancement of
429 atmospheric dilution and chemical removal by OH radicals (*De Gouw et al., 2018*). The
430 mixing ratios of formic acid poorly correlated (R^2 ranged between 0.16-0.28) with those
431 of CO (a typical tracer of combustion sources) at the five altitudes but well correlated
432 (R^2 ranged between 0.67-0.75) with those of Ox (O_3+NO_2 , a conserved metric of ozone
433 by removing NO titration effect), as shown in Figure 6. These results further confirm
434 that ambient concentrations of formic acid in urban Beijing were dominantly
435 contributed by secondary sources associated with photochemical reactions rather than
436 primary emissions.

437 Another observed evidence for the dominant contribution of formic acid from
438 secondary formations is its positive vertical gradients in nighttime (defined as the
439 period of 22:00-5:00 LT), as shown in Figure 7. Large amounts of formic acid will

440 accumulate near the surface with strong negative vertical gradients if primary emissions
441 dominate its contributions, as manifested by vertical toluene profiles. At nighttime, the
442 mixing ratios of ozone also increased with height due to enhanced removal by NO
443 titration and surface dry deposition. The deposition of formic acid was also enhanced
444 near the surface, driving the formation of positive gradients in vertical formic acid
445 profiles.

446 A notable difference existed between the diurnal variation patterns of ozone and
447 formic acid above the ground. As shown in Figure 5, the mean mixing ratios of ozone
448 at 5 m rapidly increased from 21.5 ppb_y to 36.0 ppb_y from 6:00 to 10:00 LT, while the
449 mean mixing ratios of ozone at 320 m slightly increased from 16.3 ppbv to 16.9 ppbv
450 during the same period. The enhancement rate is defined as the average change rate of
451 the species concentration between two adjacent hours. As shown in Figure 8, the ~~growth~~
452 ~~rate~~enhancement rates of ozone mixing ratios between 6:00 and 10:00 LT decreased
453 with the increase in height. This phenomenon indicates relatively weak photochemical
454 ozone formation in urban regions aloft before 10:00 LT due to the lack of reactive ozone
455 precursors (e.g., unsaturated hydrocarbons and NO_x). With the enhancement of the
456 vertical exchange of air masses with the rise of the boundary layer, large amounts of
457 ozone precursors (e.g., the observed peaks of toluene mixing ratios at 320 m at 10:00
458 LT) emitted from surface sources were transported upward and drove the formation of
459 ozone in high altitudes. In contrast to ozone, the mixing ratios of formic acid at the five
460 altitudes all increased rapidly between 6:00 and 10:00 LT. The ~~growth rate~~enhancement
461 rate of formic acid mixing ratios between 6:00 and 10:00 LT kept nearly constant below
462 320 m (Figure 8). This result implies that the oxidation products of VOCs over
463 nighttime or in the daytime before are important precursors of formic acid and can drive
464 the rapid formation of formic acid with further photooxidation. This speculation can be
465 supported by the vertical and diurnal variations of methyl vinyl ketone (MVK),
466 methacrolein (MACR), and formaldehyde, which are reported key precursors of formic
467 acid as shown in Figure 5(d) and 5(e). The diurnal variation patterns of MVK+MACR

468 and formaldehyde at the five latitudes were nearly the same with the enhancements in
469 daytime. In addition, concentrations of MVK+MACR and formaldehyde all increased
470 with height in nighttime and early morning periods, facilitating the photochemical
471 formation of formic acid even in the residual layer.

472 As a reactive hydrocarbon species, the mixing ratios of toluene rapidly decreased
473 with height in daytime (defined as the period of 11:00-16:00 LT, as shown in Figure 7)
474 due to the combined effects of atmospheric dilution and OH-initiated chemical removal.
475 By contrast, the mixing ratios of ozone and formic acid increased with height. The
476 mixing ratios of ozone and formic acid all rapidly increased with height below 102 m,
477 predominantly attributed to the reduced effect of surface dry deposition with the
478 increase in height. The mean mixing ratios of formic acid increased by 18% from 102
479 m to 320 m in daytime, while ozone mixing ratios were well mixed above 102 m. [Our
480 results point to the likely importance of photochemistry as a source of formic acid that
481 is enhanced with increasing height within the boundary layer.](#) ~~These observed results
482 support the speculation that photochemical formations of formic acid were substantially
483 enhanced with the increase in height within the boundary layer.~~

484 The precursors and formation mechanisms of atmospheric formic acid have been
485 extensively investigated in previous studies but still remain uncertain. Isoprene has long
486 been recognized as an important precursor of formic acid through reactions with O₃ and
487 OH radicals (*Neeb et al., 1997; Paulot et al., 2009*). Recent studies also found that the
488 degradation of organic aerosols (OA) derived from isoprene is an important source of
489 formic acid (*Cope et al., 2021; Bates et al., 2023*). In addition, the photooxidation of
490 other biogenic and anthropogenic hydrocarbons is also a key source of formic acid
491 (*Paulot et al., 2011; Millet et al., 2015; Link et al., 2021*). Figure 9 illustrates the mean
492 vertical profiles of several key precursors of formic acid in daytime. The concentrations
493 of isoprene and toluene (Figure 7) all decreased rapidly with height. By contrast, MVK
494 and MACR, the primary oxidation products of isoprene (*Grosjean et al., 1993*),
495 exhibited weak vertical gradients. Formaldehyde, a more general photooxidation

496 product of VOCs, exhibited similar vertical distribution patterns to those of ozone.
497 Large amounts of OVOCs were produced and accumulated in higher altitudes through
498 the oxidation of hydrocarbons and the further oxidation of some OVOCs during their
499 upward mixing course. MVK, MACR, and formaldehyde are also key precursors of
500 formic acid. MVK and MACR can react with O₃ to produce formic acid (*Link et al.*,
501 2020). Formaldehyde can be converted to methanediol in cloud droplets and then be
502 rapidly oxidized by OH to produce formic acid (*Franco et al.*, 2021). In addition, enol
503 (*Lei et al.*, 2020) and many other OVOCs (such as glycolaldehyde (*Butkovskaya et al.*,
504 2006a) and hydroxyacetone (*Butkovskaya et al.*, 2006b) can be further oxidized to
505 produce formic acid. Therefore, high concentrations of OVOCs aloft may be the
506 dominant factor that largely enhances the photochemical formation of formic acid in
507 urban regions.

508 As discussed above, formic acid exhibited strong positive vertical gradients
509 throughout the day, implying that the concentrations of formic acid measured at ground
510 level were not capable of accurately characterizing its abundance and temporal
511 variability in the whole boundary layer. Besides, the formic acid formed in daytime and
512 retained in the nocturnal residual layer also has vital impacts on the budget of formic
513 acid in the boundary layer. Thus, we used the column-integrated concentration (CIC)
514 of formic acid (the sum of the abundance in both the nocturnal residual layer and the
515 boundary layer, see detailed definitions in SI) to further clarify the diurnal variability
516 in the abundance of formic acid in the boundary layer.

517 [As shown in Figure 10](#), ~~As shown in Figure 4(f)~~, the CICs of formic acid had a
518 flatter diurnal pattern in comparison to those at ground level. The CICs of formic acid
519 had approximately stable values overnight and reached a maximum at 16:00 LT. The
520 ratio of the maximum and minimum of CIC for formic acid was only 1.3, while it was
521 4.2 for the concentrations of formic acid at 5 m. These results imply that the removal
522 of atmospheric formic acid (e.g., surface deposition and various chemical reactions)
523 may be highly overestimated if only ground-level measurements were used or

524 constrained in numerical models. The budget of the formic acid in high altitudes in the
525 boundary layer was distinctly different from those near the surface. As the result,
526 numerical models cannot accurately reproduce the abundances and budgets of formic
527 acid without the constraints of vertical observations and the clarification of formic acid
528 formation mechanisms.

529 **3.3. Vertical variations and sources of isocyanic acid**

530 The mixing ratios of isocyanic acid also exhibited strong temporal variations
531 during the campaign with a mean of 0.28 ± 0.16 ppbv at 5 m and a mean of 0.43 ± 0.21
532 ppbv at 320 m, as shown in Figure 10. The mixing ratios of isocyanic acid measured
533 at the ground level in urban Beijing were approximately 10 times higher than those
534 measured in Los Angeles, USA (0.025 ppbv) (Roberts *et al.*, 2014) and Calgary, Canada
535 (0.036 ppbv) (Woodward-Massey *et al.*, 2014) but were lower than those measured in
536 other regions in China. For example, the mean mixing ratio of isocyanic acid was 0.37
537 ppbv at a rural site (Gucheng) in the North China Plain (NCP), and 0.46 ppbv in urban
538 Guangzhou in the Pearl River Delta (PRD) region (Wang *et al.*, 2020). Isocyanic acid
539 will pose a threat to human health when its ambient mixing ratios exceed 1.0 ppbv. In
540 this study, isocyanic acid mixing ratios greater than 1.0 ppbv were not observed at
541 ground level but were observed at 320 m on three days. The maximum hourly mixing
542 ratios of isocyanic acid at 320 m reached 1.63 ppbv at 16:00 LT on July 8th.

543 The mixing ratios of isocyanic acid at the five altitudes exhibited similar diurnal
544 variation patterns. After sunrise, the mixing ratios of isocyanic acid at the five altitudes
545 all simultaneously increased and peaked at about 14:00 LT. Then, isocyanic acid mixing
546 ratios decreased slowly and reached the minimum before sunrise the following day.
547 This diurnal variation pattern of isocyanic acid measured at the ground level in urban
548 Beijing was not consistent with those measured at the Gucheng site in NCP (Wang *et al.*
549 *et al.*, 2020). The isocyanic acid mixing ratios at the Gucheng site exhibited insignificant
550 diurnal variability throughout the day with only a weak morning peak, predominantly
551 attributed to the enhancement of primary emissions. However, the diurnal variation

552 patterns of isocyanic acid measured at the five altitudes were well correlated with the
553 change in solar irradiance and were consistent with those measured at the two sites in
554 PRD. These results imply that ambient concentrations of isocyanic acid in urban Beijing
555 were mainly contributed by secondary sources associated with photochemical reactions.

556 Similar to formic acid, the simultaneous increase of isocyanic acid mixing ratios
557 at the five altitudes with the onset of sunlight also indicates the presence of adequate
558 precursors even in the nocturnal residual layer. In addition, the diurnal variability of
559 isocyanic acid mixing ratios measured below 200 m was much weaker than those
560 measured at 320 m. For example, the ratio of the daily maximum to the daily minimum
561 mixing ratios of isocyanic acid was 1.9 at 320 m, while the ratio was only 1.4 at 5 m.
562 The mean ~~growth rate~~[enhancement rate](#) of isocyanic acid mixing ratios at 320 m (0.05
563 ppbv h⁻¹) between 6:00 and 10:00 LT was approximately five times larger than that at
564 5 m (0.01 ppbv h⁻¹). The vertical gradients of isocyanic acid between 102 and 320 m
565 were also larger than those below (Figure [H12](#)). The rapid increase in both
566 concentrations and ~~growth rate~~[enhancement rates](#) of isocyanic acid with height (Figures
567 8 and [H12](#)) implies the enhanced photochemical formation of isocyanic acid in the
568 middle and upper part of the boundary layer.

569 Secondary formation precursors of atmospheric isocyanic acid were still poorly
570 understood so far. Amides were considered important precursors of isocyanic acid
571 (*Roberts et al., 2014; Rosanka et al., 2020*). As reported in our previous study (*Wang*
572 *et al., 2020*), C₃ amides accounted for the largest fraction of the total concentrations of
573 amides and were dominant contributors to the secondary formation of isocyanic acid.
574 The mixing ratios of C₃ amides in Guangzhou in PRD exhibited strong diurnal
575 variations. Along with the sunrise, the mixing ratios of C₃ amides rapidly decreased and
576 reached the minimum at 13:00 LT. Afterward, the mixing ratios of C₃ amides started to
577 increase and accumulated at night. [As shown in Figure S4, the influence of long tubing](#)
578 [on the measurement of amides was limited, so we also measured the amides during the](#)
579 [field campaign](#). However, the mixing ratios of C₃ amides in Beijing and Gucheng in

580 NCP exhibited insignificant diurnal variability, consistent with those of isocyanic acid.
581 The mean mixing ratios of C₃ amides at 5 m in urban Beijing is only 0.03 ppbv during
582 the campaign, which is one order of magnitude lower than those in Guangzhou (0.35
583 ppbv) and Gucheng (0.18 ppbv). The mixing ratios of C₃ amides measured at the five
584 altitudes in urban Beijing were also approximately one order of magnitude lower than
585 those of isocyanic acid (Figure 412). Besides, the mixing ratios of C₃ amides decreased
586 with height in both nighttime and daytime, indicating predominant contributions from
587 primary emissions. This is consistent with the fact that primary emissions of chemical
588 composition from industry-related sources have been largely reduced with the outward
589 migration of industry in urban Beijing. By contrast, the mixing ratios of isocyanic acid
590 increased with height in both day and night with an average of 0.32 ppbv at 5 m and
591 0.60 ppbv at 320 m. These results suggest that C₃ amides were far more enough to
592 account for the secondary formation of isocyanic acid in urban Beijing.

593 Figure 4213(a) gives the composition and average concentrations of C₁-C₁₀
594 amides measured at the five altitudes during the campaign. C₂ amides accounted for the
595 largest fraction of the total mixing ratios of amides. The total mixing ratios of amides
596 exhibited decreasing tendencies with the increase in height, suggesting predominant
597 contributions from direct emissions of surface sources. As for formamide, its mixing
598 ratios exhibited an increasing tendency from 0.024 ppbv at 5 m to 0.030 ppbv at 320 m.
599 The positive vertical gradients of formamide suggest its enhanced formation with
600 height, probably due to the enhancements of formic acid. However, the average
601 concentration ratios of formamide to formic acid slightly varied between 0.01 and 0.02
602 among the five heights. The average concentration ratios of formamide to isocyanic
603 acid decreased from 0.09 at 5 m to 0.07 at 320 m. These results imply that the formation
604 of isocyanic acid through the pathway of HCOOH-CH₃NO-HNCO may be enhanced
605 with the increase in height but could only contribute a tiny fraction of the observed
606 isocyanic acid, as shown in Figure 4213(b). Assuming the full conversion of C₁-C₁₀
607 amides to isocyanic acid, the average concentration ratios of amides (sum of C₁-C₁₀) to

608 isocyanic acid below 320 m only ranged between 0.32 and 0.56 and decreased with
609 height. Therefore, in addition to amides, there must be other important precursors and
610 formation pathways of isocyanic acid, particularly in high altitudes. The simultaneous
611 increase of isocyanic acid concentrations at the five heights upon sunrise (Figure 1011)
612 implies the presence of adequate precursors in the nocturnal residual layer. The
613 oxidation products of VOCs driven by ozone and NO₃ radicals in nighttime may be an
614 important class of precursors. In addition, the largest ~~growth rate~~ enhancement rates and
615 highest concentrations of isocyanic acid at 320 m in daytime also suggest that high
616 concentrations of OVOCs and low-NO_x conditions may enhance the secondary
617 formation of isocyanic acid.

618 The positive vertical gradients of isocyanic acid imply that the secondary
619 formation of isocyanic acid aloft could serve as an important source of surface isocyanic
620 acid in daytime driven by turbulence mixing. The CICs of isocyanic acid were
621 calculated to further clarify its abundance and temporal variability in the whole
622 boundary layer. Distinct diurnal patterns were observed between the ground-level
623 concentrations and CICs of isocyanic acid. Analogous to formic acid, the CICs of
624 isocyanic acid varied insignificantly over nighttime and enhanced in daytime, reaching
625 the maximum at approximately 14:00 LT. The formation of some chemicals can be
626 largely enhanced at higher altitudes and so using ground-level measurements to
627 constrain numerical models may be not adequate. ~~Therefore, the problems of formic~~
628 ~~acid caused by the limitations of ground-level observations also raised for isocyanic~~
629 ~~acid.~~

630 **4. Conclusion**

631 In this study, vertical and diurnal variations of formic and isocyanic acids in
632 urban Beijing were investigated using tower-based online gradient measurements. The
633 measurements of isocyanic acid can be well measured through long PFA Teflon tubes.
634 The measurements of formic acid made through long tubes were slightly influenced by

635 [the memory effect of tubing walls, and the vertical increasing gradients of formic acid](#)
636 [may be slightly enhanced if the tubing effects were considered.](#) ~~The measurements of~~
637 ~~formic acid made through long tubes were slightly influenced by the memory effect of~~
638 ~~tubing walls but had minor impacts on analyzing its vertical distributions.~~ The
639 concentrations of formic and isocyanic acids all increased with height in both nighttime
640 and daytime. The diurnal and vertical distribution patterns of formic and isocyanic acids
641 all suggest that their abundances in the boundary layer were dominantly contributed by
642 secondary formation associated with photochemical reactions. The photochemical
643 formations of formic and isocyanic acids were also substantially enhanced with the
644 increase in height. The formation pathway of isocyanic acid through $\text{HCOOH-CH}_3\text{NO-}$
645 HNCO only accounted for a tiny fraction of its ambient abundance. The formic and
646 isocyanic acids photochemically formed in the middle and upper parts of the boundary
647 layer were important sources for those at ground level in urban region. The differences
648 of the diurnal patterns between CICs and ground-level concentrations of formic and
649 isocyanic acids further highlight the importance of vertical observations in elucidating
650 their budgets and sources in the whole boundary layer.

651 Characterization of the vertical variations in formic and isocyanic acids could
652 provide valuable information for elucidating their budgets and sources in the boundary
653 layer. However, there are still many important but unresolved questions associated with
654 the vertical distributions of formic and isocyanic acids. For example, the key precursors
655 that drive the rapid formation of formic and isocyanic acids in the residual layer are still
656 unknown. Are there any changes in the key precursors and formation pathways of
657 formic and isocyanic acids with the increase of height in urban region? To answer these
658 questions, the combination of vertical gradient measurements of more chemical species
659 and numerical simulations is needed in future studies.

660 **Supporting Information:** Additional experimental details, materials, and methods,
661 including schematic illustration of tubing test, determination of the long tubes'
662 cumulative influence, and calculation of CICs.

663 **Data availability**

664 Data related to this article are available online at
665 <https://doi.org/10.7910/DVN/ANH0WE>.

666 **Author contributions**

667 QY, XBL, BY, and YH designed the research. QY, XBL, BY, XZ, YH, LY, XH,
668 JQ and MS contributed to the data collection and data analysis. QY and XBL wrote the
669 paper with contributions from all coauthors. All the coauthors discussed the results and
670 reviewed the paper.

671 **Competing interests**

672 The authors declare that they have no conflict of interest.

673 **Acknowledgment**

674 This work was financially supported by the National Key R&D Plan of China
675 (grant No. 2023YFC3706103, 2023YFC3706201, 2022YFC3700604) and the National
676 Natural Science Foundation of China (grant No. 42121004, 42275103, [42205904](#),
677 42230701, 42305095). This work was also supported by the Special Fund Project for
678 Science and Technology Innovation Strategy of Guangdong Province (Grant No.
679 2019B121205004). The authors would like to thank the personnel who participated in
680 data collection, instrument maintenance, and logistic support during the field campaign.

681 **Reference**

682 Acton, W. J. F., Huang, Z., Davison, B., Drysdale, W. S., Fu, P., Hollaway, M., Langford,
683 B., Lee, J., Liu, Y., Metzger, S., Mullinger, N., Nemitz, E., Reeves, C. E., Squires, F.
684 A., Vaughan, A. R., Wang, X., Wang, Z., Wild, O., Zhang, Q., Zhang, Y., and Hewitt,
685 C. N.: Surface–atmosphere fluxes of volatile organic compounds in Beijing,

686 Atmospheric Chemistry and Physics, 20, 15101-15125, 10.5194/acp-20-15101-2020,
687 2020.

688 Alwe, H. D., Millet, D. B., Chen, X., Raff, J. D., Payne, Z. C., and Fledderman, K.:
689 Oxidation of Volatile Organic Compounds as the Major Source of Formic Acid in a
690 Mixed Forest Canopy, *Geophysical Research Letters*, 46, 2940-2948,
691 <https://doi.org/10.1029/2018GL081526>, 2019.

692 Andreae, M. O., Talbot, R. W., Andreae, T. W., and Harriss, R. C.: Formic and acetic
693 acid over the central Amazon region, Brazil: 1. Dry season, *Journal of Geophysical*
694 *Research: Atmospheres*, 93, 1616-1624, <https://doi.org/10.1029/JD093iD02p01616>,
695 1988.

696 Bannan, T. J., Bacak, A., Muller, J. B. A., Booth, A. M., Jones, B., Le Breton, M.,
697 Leather, K. E., Ghalaieny, M., Xiao, P., Shallcross, D. E., and Percival, C. J.:
698 Importance of direct anthropogenic emissions of formic acid measured by a chemical
699 ionisation mass spectrometer (CIMS) during the Winter ClearfLo Campaign in
700 London, January 2012, *Atmospheric Environment*, 83, 301-310,
701 10.1016/j.atmosenv.2013.10.029, 2014.

702 Bannan, T. J., Murray Booth, A., Le Breton, M., Bacak, A., Muller, J. B. A., Leather, K.
703 E., Khan, M. A. H., Lee, J. D., Dunmore, R. E., Hopkins, J. R., Fleming, Z. L., Sheps,
704 L., Taatjes, C. A., Shallcross, D. E., and Percival, C. J.: Seasonality of Formic Acid
705 (HCOOH) in London during the ClearfLo Campaign, *Journal of Geophysical*
706 *Research: Atmospheres*, 122, 10.1002/2017jd027064, 2017.

707 Barnes, I., Solignac, G., Mellouki, A., and Becker, K. H.: Aspects of the atmospheric
708 chemistry of amides, *ChemPhyChem*, 11, 3844-3857, 10.1002/cphc.201000374,
709 2010.

710 Bates, K. H., Jacob, D. J., Cope, J. D., Chen, X., Millet, D. B., and Nguyen, T. B.:
711 Emerging investigator series: aqueous oxidation of isoprene-derived organic aerosol
712 species as a source of atmospheric formic and acetic acids, *Environmental Science:*
713 *Atmospheres*, 10.1039/d3ea00076a, 2023.

714 Benish, S. E., He, H., Ren, X., Roberts, S. J., Salawitch, R. J., Li, Z., Wang, F., Wang,
715 Y., Zhang, F., Shao, M., Lu, S., and Dickerson, R. R.: Measurement report: Aircraft
716 observations of ozone, nitrogen oxides, and volatile organic compounds over Hebei
717 Province, China, *Atmospheric Chemistry and Physics*, 20, 14523-14545,
718 10.5194/acp-20-14523-2020, 2020.

719 Borduas, N., Murphy, J. G., Wang, C., Silva, G. d., Abbatt, J. P. D. J. E. S., and Letters,
720 T.: Gas Phase Oxidation of Nicotine by OH Radicals: Kinetics, Mechanisms, and
721 Formation of HNCO, 3, 327-331, 2016.

722 Butkovskaya, N. I., Pouvesle, N., Kukui, A., and Le Bras, G.: Mechanism of the OH-
723 Initiated Oxidation of Glycolaldehyde over the Temperature Range 233–296 K, *The*
724 *Journal of Physical Chemistry A*, 110, 13492-13499, 10.1021/jp064993k, 2006a.

725 Butkovskaya, N. I., Pouvesle, N., Kukui, A., Mu, Y., and Le Bras, G.: Mechanism of
726 the OH-Initiated Oxidation of Hydroxyacetone over the Temperature Range 236–298
727 K, *The Journal of Physical Chemistry A*, 110, 6833-6843, 10.1021/jp056345r, 2006b.

728 Chandra, B. P. and Sinha, V.: Contribution of post-harvest agricultural paddy residue
729 fires in the N.W. Indo-Gangetic Plain to ambient carcinogenic benzenoids, toxic
730 isocyanic acid and carbon monoxide, *Environment International*, 88, 187-197,
731 10.1016/j.envint.2015.12.025, 2016.

732 Chebbi, A. and Carlier, P.: Carboxylic acids in the troposphere, occurrence, sources,
733 and sinks: A review, *Atmospheric Environment*, 30, 4233-4249,
734 [https://doi.org/10.1016/1352-2310\(96\)00102-1](https://doi.org/10.1016/1352-2310(96)00102-1), 1996.

735 Cope, J. D., Abellar, K. A., Bates, K. H., Fu, X., and Nguyen, T. B.: Aqueous
736 Photochemistry of 2-Methyltetrol and Erythritol as Sources of Formic Acid and
737 Acetic Acid in the Atmosphere, *ACS Earth and Space Chemistry*, 5, 1265-1277,
738 10.1021/acsearthspacechem.1c00107, 2021.

739 De Gouw, J. A., Gilman, J. B., Kim, S. W., Alvarez, S. L., Dusanter, S., Graus, M.,
740 Griffith, S. M., Isaacman - VanWertz, G., Kuster, W. C., Lefer, B. L., Lerner, B. M.,
741 McDonald, B. C., Rappenglück, B., Roberts, J. M., Stevens, P. S., Stutz, J., Thalman,
742 R., Veres, P. R., Volkamer, R., Warneke, C., Washenfelder, R. A., and Young, C. J.:
743 Chemistry of Volatile Organic Compounds in the Los Angeles Basin: Formation of
744 Oxygenated Compounds and Determination of Emission Ratios, *Journal of
745 Geophysical Research: Atmospheres*, 123, 2298-2319, 10.1002/2017jd027976, 2018.

746 Deming, B. L., Pagonis, D., Liu, X., Day, D. A., Talukdar, R., Krechmer, J. E., de Gouw,
747 J. A., Jimenez, J. L., and Ziemann, P. J.: Measurements of delays of gas-phase
748 compounds in a wide variety of tubing materials due to gas-wall interactions,
749 *Atmospheric Measurement Techniques*, 12, 3453-3461, 10.5194/amt-12-3453-2019,
750 2019.

751 Enders, G., Dlugi, R., Steinbrecher, R., Clement, B., Daiber, R., Eijk, J. v., Gäb, S.,
752 Haziza, M., Helas, G., Herrmann, U., Kessel, M., Kesselmeier, J., Kotzias, D.,
753 Kourtidis, K., Kurth, H. H., McMillen, R. T., Roider, G., Schürmann, W., Teichmann,
754 U., and Torres, L.: Biosphere/Atmosphere interactions: Integrated research in a
755 European coniferous forest ecosystem, *Atmospheric Environment*, 26, 171-189,
756 [https://doi.org/10.1016/0960-1686\(92\)90269-Q](https://doi.org/10.1016/0960-1686(92)90269-Q), 1992.

757 Fang, X., Shao, M., Stohl, A., Zhang, Q., Zheng, J., Guo, H., Wang, C., Wang, M., Ou,
758 J., Thompson, R. L., and Prinn, R. G.: Top-down estimates of benzene and toluene
759 emissions in the Pearl River Delta and Hong Kong, China, *Atmospheric Chemistry
760 and Physics*, 16, 3369-3382, 10.5194/acp-16-3369-2016, 2016.

761 Franco, B., Blumenstock, T., Cho, C., Clarisse, L., Clerbaux, C., Coheur, P. F., De
762 Mazière, M., De Smedt, I., Dorn, H. P., Emmerichs, T., Fuchs, H., Gkatzelis, G.,
763 Griffith, D. W. T., Gromov, S., Hannigan, J. W., Hase, F., Hohaus, T., Jones, N.,
764 Kerkweg, A., Kiendler-Scharr, A., Lutsch, E., Mahieu, E., Novelli, A., Ortega, I.,
765 Paton-Walsh, C., Pommier, M., Pozzer, A., Reimer, D., Rosanka, S., Sander, R.,
766 Schneider, M., Strong, K., Tillmann, R., Van Roozendaal, M., Vereecken, L.,
767 Vigouroux, C., Wahner, A., and Taraborrelli, D.: Ubiquitous atmospheric production
768 of organic acids mediated by cloud droplets, *Nature*, 593, 233-237, 10.1038/s41586-
769 021-03462-x, 2021.

770 Fulgham, S. R., Brophy, P., Link, M., Ortega, J., Pollack, I., and Farmer, D. K.: Seasonal
771 Flux Measurements over a Colorado Pine Forest Demonstrate a Persistent Source of
772 Organic Acids, *ACS Earth and Space Chemistry*, 3, 2017-2032,
773 10.1021/acsearthspacechem.9b00182, 2019.

774 Fulgham, S. R., Millet, D. B., Alwe, H. D., Goldstein, A. H., Schobesberger, S., and
775 Farmer, D. K.: Surface Wetness as an Unexpected Control on Forest Exchange of
776 Volatile Organic Acids, *Geophysical Research Letters*, 47, 10.1029/2020gl088745,
777 2020.

778 Galloway, J. N., Likens, G. E., Keene, W. C., and Miller, J. M.: The composition of
779 precipitation in remote areas of the world, *Journal of Geophysical Research: Oceans*,
780 87, 8771-8786, <https://doi.org/10.1029/JC087iC11p08771>, 1982.

781 Goode, J. G., Yokelson, R. J., Ward, D. E., Susott, R. A., Babbitt, R. E., Davies, M. A.,
782 and Hao, W. M.: Measurements of excess O₃, CO₂, CO, CH₄, C₂H₄, C₂H₂, HCN,
783 NO, NH₃, HCOOH, CH₃COOH, HCHO, and CH₃OH in 1997 Alaskan biomass
784 burning plumes by airborne Fourier transform infrared spectroscopy (AFTIR),
785 *Journal of Geophysical Research: Atmospheres*, 105, 22147-22166,
786 10.1029/2000jd900287, 2000.

787 Grosjean, D., Williams, E. L., II, and Grosjean, E.: Atmospheric chemistry of isoprene
788 and of its carbonyl products, *Environmental Science & Technology*, 27, 830-840,
789 10.1021/es00042a004, 1993.

790 Helmig, D., Johnson, B., Oltmans, S., Neff, W., Eisele, F., and Davis, D.: Elevated
791 ozone in the boundary layer at South Pole, *Atmospheric Environment*, 42, 2788-2803,
792 10.1016/j.atmosenv.2006.12.032, 2008a.

793 Helmig, D., Johnson, B., Warshawsky, M., Morse, T., Neff, W., Eisele, F., and Davis,
794 D.: Nitric oxide in the boundary-layer at South Pole during the Antarctic
795 Tropospheric Chemistry Investigation (ANTCI), *Atmospheric Environment*, 42,
796 2817-2830, 10.1016/j.atmosenv.2007.03.061, 2008b.

797 Hems, R. F., Wang, C., Collins, D. B., Zhou, S., Borduas-Dedekind, N., Siegel, J. A.,
798 and Abbatt, J. P. D.: Sources of isocyanic acid (HNCO) indoors: a focus on cigarette
799 smoke, *Environmental Science: Processes & Impacts*, 21, 1334-1341,
800 10.1039/c9em00107g, 2019.

801 Hu, L., Millet, D. B., Kim, S. Y., Wells, K. C., Griffis, T. J., Fischer, E. V., Helmig, D.,
802 Hueber, J., and Curtis, A. J.: North American acetone sources determined from tall
803 tower measurements and inverse modeling, *Atmospheric Chemistry and Physics*, 13,
804 3379-3392, 10.5194/acp-13-3379-2013, 2013.

805 Hu, X., Yang, G., Liu, Y., Lu, Y., Wang, Y., Chen, H., Chen, J., and Wang, L.:
806 Atmospheric gaseous organic acids in winter in a rural site of the North China Plain,
807 *Journal of Environmental Sciences*, 113, 190-203, 10.1016/j.jes.2021.05.035, 2022.

808 Jacob, D. J.: Chemistry of OH in remote clouds and its role in the production of formic
809 acid and peroxymonosulfate, *Journal of Geophysical Research: Atmospheres*, 91,
810 9807-9826, <https://doi.org/10.1029/JD091iD09p09807>, 1986.

811 Jaisson, S., Pietrement, C., and Gillery, P.: Carbamylation-derived products: bioactive

812 compounds and potential biomarkers in chronic renal failure and atherosclerosis,
813 *Clinical chemistry*, 57, 1499-1505, 10.1373/clinchem.2011.163188, 2011.

814 Jathar, S. H., Heppding, C., Link, M. F., Farmer, D. K., Akherati, A., Kleeman, M. J.,
815 de Gouw, J. A., Veres, P. R., and Roberts, J. M.: Investigating diesel engines as an
816 atmospheric source of isocyanic acid in urban areas, *Atmospheric Chemistry and*
817 *Physics*, 17, 8959-8970, 10.5194/acp-17-8959-2017, 2017.

818 Ji, Y., Huey, L. G., Tanner, D. J., Lee, Y. R., Veres, P. R., Neuman, J. A., Wang, Y., and
819 Wang, X.: A vacuum ultraviolet ion source (VUV-IS) for iodide-chemical ionization
820 mass spectrometry: a substitute for radioactive ion sources, *Atmospheric*
821 *Measurement Techniques*, 13, 3683-3696, 10.5194/amt-13-3683-2020, 2020.

822 Karion, A., Sweeney, C., Tans, P., and Newberger, T.: AirCore: An Innovative
823 Atmospheric Sampling System, *Journal of Atmospheric and Oceanic Technology*, 27,
824 1839-1853, 10.1175/2010jtecha1448.1, 2010.

825 Kawamura, K. and Kaplan, I. R.: Organic compounds in the rainwater of Los Angeles,
826 *Environmental Science & Technology*, 17, 497-501, 10.1021/es00114a011, 1983.

827 Kawamura, K., Steinberg, S., and Kaplan, I. R.: Homologous series of C1-C10
828 monocarboxylic acids and C1-C6 carbonyls in Los Angeles air and motor vehicle
829 exhausts, *Atmospheric Environment*, 34, 4175-4191, [https://doi.org/10.1016/S1352-](https://doi.org/10.1016/S1352-2310(00)00212-0)
830 [2310\(00\)00212-0](https://doi.org/10.1016/S1352-2310(00)00212-0), 2000.

831 Keene, W. C. and Galloway, J. N.: Organic acidity in precipitation of North America,
832 *Atmospheric Environment*, 18, 2491-2497, [https://doi.org/10.1016/0004-](https://doi.org/10.1016/0004-6981(84)90020-9)
833 [6981\(84\)90020-9](https://doi.org/10.1016/0004-6981(84)90020-9), 1984.

834 Kesselmeier, J., Bode, K., Gerlach, C., and Jork, E. M.: Exchange of atmospheric
835 formic and acetic acids with trees and crop plants under controlled chamber and
836 purified air conditions, *Atmospheric Environment*, 32, 1765-1775,
837 [https://doi.org/10.1016/S1352-2310\(97\)00465-2](https://doi.org/10.1016/S1352-2310(97)00465-2), 1998.

838 Khare, P., Kumar, N., Kumari, K. M., and Srivastava, S. S.: Atmospheric formic and
839 acetic acids: An overview, *Reviews of Geophysics*, 37, 227-248,
840 <https://doi.org/10.1029/1998RG900005>, 1999.

841 Koeth, R. A., Kalantar-Zadeh, K., Wang, Z., Fu, X., Tang, W. H., and Hazen, S. L.:
842 Protein carbamylation predicts mortality in ESRD, *Journal of the American Society*
843 *of Nephrology*, 24, 853-861, 10.1681/ASN.2012030254, 2013.

844 Krechmer, J. E., Day, D. A., Ziemann, P. J., and Jimenez, J. L.: Direct Measurements
845 of Gas/Particle Partitioning and Mass Accommodation Coefficients in
846 Environmental Chambers, *Environmental science & technology*, 51, 11867-11875,
847 10.1021/acs.est.7b02144, 2017.

848 Le Breton, M., Bacak, A., Muller, J. B. A., Xiao, P., Shallcross, B. M. A., Batt, R.,
849 Cooke, M. C., Shallcross, D. E., Bauguitte, S. J. B., and Percival, C. J.: Simultaneous
850 airborne nitric acid and formic acid measurements using a chemical ionization mass
851 spectrometer around the UK: Analysis of primary and secondary production
852 pathways, *Atmospheric Environment*, 83, 166-175, 10.1016/j.atmosenv.2013.10.008,
853 2014.

854 Lei, X., Wang, W., Gao, J., Wang, S., and Wang, W.: Atmospheric Chemistry of Enols:
855 The Formation Mechanisms of Formic and Peroxyformic Acids in Ozonolysis of
856 Vinyl Alcohol, *The Journal of Physical Chemistry A*, 124, 4271-4279,
857 10.1021/acs.jpca.0c01480, 2020.

858 Li, T., Wang, Z., Yuan, B., Ye, C., Lin, Y., Wang, S., Sha, Q. e., Yuan, Z., Zheng, J., and
859 Shao, M.: Emissions of carboxylic acids, hydrogen cyanide (HCN) and isocyanic
860 acid (HNCO) from vehicle exhaust, *Atmospheric Environment*, 247,
861 10.1016/j.atmosenv.2021.118218, 2021.

862 Li, X.-B., Yuan, B., Wang, S., Wang, C., Lan, J., Liu, Z., Song, Y., He, X., Huangfu, Y.,
863 Pei, C., Cheng, P., Yang, S., Qi, J., Wu, C., Huang, S., You, Y., Chang, M., Zheng, H.,
864 Yang, W., Wang, X., and Shao, M.: Variations and sources of volatile organic
865 compounds (VOCs) in urban region: insights from measurements on a tall tower,
866 *Atmospheric Chemistry and Physics*, 22, 10567-10587, 10.5194/acp-22-10567-2022,
867 2022.

868 Li, X., Zhang, C., Liu, A., Yuan, B., Yang, H., Liu, C., Wang, S., Huangfu, Y., Qi, J.,
869 Liu, Z., He, X., Song, X., Chen, Y., Peng, Y., Zhang, X., Zheng, E., Yang, L., Yang,
870 Q., Qin, G., Zhou, J., and Shao, M.: Assessment of Long Tubing in Measuring
871 Atmospheric Trace Gases: Applications on Tall Towers, *Environmental Science:
872 Atmospheres*, 506-520, 10.1039/d2ea00110a, 2023.

873 Liggio, J., Moussa, S. G., Wentzell, J., Darlington, A., Liu, P., Leithead, A., Hayden, K.,
874 O'Brien, J., Mittermeier, R. L., Staebler, R., Wolde, M., and Li, S.-M.: Understanding
875 the primary emissions and secondary formation of gaseous organic acids in the oil
876 sands region of Alberta, Canada, *Atmospheric Chemistry and Physics*, 17, 8411-8427,
877 10.5194/acp-17-8411-2017, 2017.

878 Link, M. F., Brophy, P., Fulgham, S. R., Murschell, T., and Farmer, D. K.: Isoprene
879 versus Monoterpenes as Gas-Phase Organic Acid Precursors in the Atmosphere, *ACS
880 Earth and Space Chemistry*, 5, 1600-1612, 10.1021/acsearthspacechem.1c00093,
881 2021.

882 Link, M. F., Nguyen, T. B., Bates, K., Müller, J.-F., and Farmer, D. K.: Can Isoprene
883 Oxidation Explain High Concentrations of Atmospheric Formic and Acetic Acid over
884 Forests?, *ACS Earth and Space Chemistry*, 4, 730-740,
885 10.1021/acsearthspacechem.0c00010, 2020.

886 Liu, X., Deming, B., Pagonis, D., Day, D. A., Palm, B. B., Talukdar, R., Roberts, J. M.,
887 Veres, P. R., Krechmer, J. E., Thornton, J. A., de Gouw, J. A., Ziemann, P. J., and
888 Jimenez, J. L.: Effects of gas-wall interactions on measurements of semivolatile
889 compounds and small polar molecules, *Atmospheric Measurement Techniques*, 12,
890 3137-3149, 10.5194/amt-12-3137-2019, 2019.

891 Lopez-Hilfiker, F. D., Mohr, C., Ehn, M., Rubach, F., Kleist, E., Wildt, J., Mentel, T. F.,
892 Lutz, A., Hallquist, M., Worsnop, D., and Thornton, J. A.: A novel method for online
893 analysis of gas and particle composition: description and evaluation of a Filter Inlet
894 for Gases and AEROSols (FIGAERO), *Atmospheric Measurement Techniques*, 7,
895 983-1001, 10.5194/amt-7-983-2014, 2014.

896 Mattila, J. M., Brophy, P., Kirkland, J., Hall, S., Ullmann, K., Fischer, E. V., Brown, S.,
897 McDuffie, E., Tevlin, A., and Farmer, D. K.: Tropospheric sources and sinks of gas-
898 phase acids in the Colorado Front Range, *Atmospheric Chemistry and Physics*, 18,
899 12315-12327, 10.5194/acp-18-12315-2018, 2018.

900 Meng, F., Qin, M., Tang, K., Duan, J., Fang, W., Liang, S., Ye, K., Xie, P., Sun, Y., Xie,
901 C., Ye, C., Fu, P., Liu, J., and Liu, W.: High-resolution vertical distribution and
902 sources of HONO and NO₂ in the nocturnal boundary layer
903 in urban Beijing, China, *Atmospheric Chemistry and Physics*, 20, 5071-5092,
904 10.5194/acp-20-5071-2020, 2020.

905 Millet, D. B., Baasandorj, M., Farmer, D. K., Thornton, J. A., Baumann, K., Brophy, P.,
906 Chaliyakunnel, S., de Gouw, J. A., Graus, M., Hu, L., Koss, A., Lee, B. H., Lopez-
907 Hilfiker, F. D., Neuman, J. A., Paulot, F., Peischl, J., Pollack, I. B., Ryerson, T. B.,
908 Warneke, C., Williams, B. J., and Xu, J.: A large and ubiquitous source of
909 atmospheric formic acid, *Atmospheric Chemistry and Physics*, 15, 6283-6304,
910 10.5194/acp-15-6283-2015, 2015.

911 Mungall, E. L., Abbatt, J. P. D., Wentzell, J. J. B., Wentworth, G. R., Murphy, J. G.,
912 Kunkel, D., Gute, E., Tarasick, D. W., Sharma, S., Cox, C. J., Uttal, T., and Liggio,
913 J.: High gas-phase mixing ratios of formic and acetic acid in the High Arctic,
914 *Atmospheric Chemistry and Physics*, 18, 10237-10254, 10.5194/acp-18-10237-2018,
915 2018.

916 Mydel, P., Wang, Z., Brisslert, M., Hellvard, A., Dahlberg, L. E., Hazen, S. L., and
917 Bokarewa, M. I. J. T. J. o. I.: Carbamylation-Dependent Activation of T Cells: A
918 Novel Mechanism in the Pathogenesis of Autoimmune Arthritis, *The Journal of*
919 *Immunology*, 184, 6882 - 6890, 2010.

920 Neeb, P., Sauer, F., Horie, O., and Moortgat, G. K.: Formation of hydroxymethyl
921 hydroperoxide and formic acid in alkene ozonolysis in the presence of water vapour,
922 *Atmospheric Environment*, 31, 1417-1423, [https://doi.org/10.1016/S1352-
923 2310\(96\)00322-6](https://doi.org/10.1016/S1352-2310(96)00322-6), 1997.

924 Pagonis, D., Krechmer, J. E., de Gouw, J., Jimenez, J. L., and Ziemann, P. J.: Effects of
925 gas-wall partitioning in Teflon tubing and instrumentation on time-resolved
926 measurements of gas-phase organic compounds, *Atmospheric Measurement*
927 *Techniques*, 10, 4687-4696, 10.5194/amt-10-4687-2017, 2017.

928 Palm, B. B., Liu, X., Jimenez, J. L., and Thornton, J. A.: Performance of a new coaxial
929 ion-molecule reaction region for low-pressure chemical ionization mass
930 spectrometry with reduced instrument wall interactions, *Atmospheric Measurement*
931 *Techniques*, 12, 5829-5844, 10.5194/amt-12-5829-2019, 2019.

932 Paulot, F., Crouse, J. D., Kjaergaard, H. G., Kroll, J. H., Seinfeld, J. H., and Wennberg,
933 P. O.: Isoprene photooxidation: new insights into the production of acids and organic
934 nitrates, *Atmospheric Chemistry and Physics*, 9, 1479-1501, 10.5194/acp-9-1479-
935 2009, 2009.

936 Paulot, F., Wunch, D., Crouse, J. D., Toon, G. C., Millet, D. B., DeCarlo, P. F.,
937 Vigouroux, C., Deutscher, N. M., Gonzalez Abad, G., Notholt, J., Warneke, T.,

938 Hannigan, J. W., Warneke, C., de Gouw, J. A., Dunlea, E. J., De Maziere, M., Griffith,
939 D. W. T., Bernath, P., Jimenez, J. L., and Wennberg, P. O.: Importance of secondary
940 sources in the atmospheric budgets of formic and acetic acids, *Atmospheric*
941 *Chemistry and Physics*, 11, 1989-2013, 10.5194/acp-11-1989-2011, 2011.

942 Roberts, J. M. and Liu, Y.: Solubility and solution-phase chemistry of isocyanic acid,
943 methyl isocyanate, and cyanogen halides, *Atmospheric Chemistry and Physics*, 19,
944 4419-4437, 10.5194/acp-19-4419-2019, 2019.

945 Roberts, J. M., Veres, P. R., Cochran, A. K., Warneke, C., Burling, I. R., Yokelson, R.
946 J., Lerner, B., Gilman, J. B., Kuster, W. C., Fall, R., and de Gouw, J.: Isocyanic acid
947 in the atmosphere and its possible link to smoke-related health effects, *Proceedings*
948 *of the National Academy of Sciences*, 108, 8966-8971, 10.1073/pnas.1103352108,
949 2011.

950 Roberts, J. M., Veres, P. R., VandenBoer, T. C., Warneke, C., Graus, M., Williams, E.
951 J., Lefer, B., Brock, C. A., Bahreini, R., Öztürk, F., Middlebrook, A. M., Wagner, N.
952 L., Dubé, W. P., and de Gouw, J. A.: New insights into atmospheric sources and sinks
953 of isocyanic acid, HNCO, from recent urban and regional observations, *Journal of*
954 *Geophysical Research: Atmospheres*, 119, 1060-1072, 10.1002/2013jd019931, 2014.

955 Rosanka, S., Vu, G. H. T., Nguyen, H. M. T., Pham, T. V., Javed, U., Taraborrelli, D.,
956 and Vereecken, L.: Atmospheric chemical loss processes of isocyanic acid (HNCO):
957 a combined theoretical kinetic and global modelling study, *Atmospheric Chemistry*
958 *and Physics*, 20, 6671-6686, 10.5194/acp-20-6671-2020, 2020.

959 Schnitzhofer, R., Wisthaler, A., and Hansel, A.: Real-time profiling of organic trace
960 gases in the planetary boundary layer by PTR-MS using a tethered balloon,
961 *Atmospheric Measurement Techniques*, 2, 773-777, 10.5194/amt-2-773-2009, 2009.

962 Schobesberger, S., Lopez - Hilfiker, F. D., Taipale, D., Millet, D. B., D'Ambro, E. L.,
963 Rantala, P., Mammarella, I., Zhou, P., Wolfe, G. M., Lee, B. H., Boy, M., and
964 Thornton, J. A.: High upward fluxes of formic acid from a boreal forest canopy,
965 *Geophysical Research Letters*, 43, 9342-9351, 10.1002/2016gl069599, 2016.

966 Skorokhod, A. I., Berezina, E. V., Moiseenko, K. B., Elansky, N. F., and Belikov, I. B.:
967 Benzene and toluene in the surface air of northern Eurasia from TROICA-12
968 campaign along the Trans-Siberian Railway, *Atmospheric Chemistry and Physics*, 17,
969 5501-5514, 10.5194/acp-17-5501-2017, 2017.

970 Stavrou, T., Müller, J. F., Peeters, J., Razavi, A., Clarisse, L., Clerbaux, C., Coheur,
971 P. F., Hurtmans, D., De Mazière, M., Vigouroux, C., Deutscher, N. M., Griffith, D.
972 W. T., Jones, N., and Paton-Walsh, C.: Satellite evidence for a large source of formic
973 acid from boreal and tropical forests, *Nature Geoscience*, 5, 26-30,
974 10.1038/ngeo1354, 2011.

975 Tan, Q., Ge, B., Xu, X., Gan, L., Yang, W., Chen, X., Pan, X., Wang, W., Li, J., and
976 Wang, Z.: Increasing impacts of the relative contributions of regional transport on air
977 pollution in Beijing: Observational evidence, *Environmental Pollution*, 292, 118407,
978 10.1016/j.envpol.2021.118407, 2022.

979 Verbrugge, F. H., Tang, W. H., and Hazen, S. L.: Protein carbamylation and

980 cardiovascular disease, *Kidney International*, 88, 474-478, 10.1038/ki.2015.166,
981 2015.

982 Veres, P. R., Roberts, J. M., Cochran, A. K., Gilman, J. B., Kuster, W. C., Holloway, J.
983 S., Graus, M., Flynn, J., Lefer, B., Warneke, C., and de Gouw, J.: Evidence of rapid
984 production of organic acids in an urban air mass, *Geophysical Research Letters*, 38,
985 L17807, 10.1029/2011gl048420, 2011.

986 Wang, Z., Nicholls, S. J., Rodriguez, E. R., Kummu, O., Horkko, S., Barnard, J.,
987 Reynolds, W. F., Topol, E. J., DiDonato, J. A., and Hazen, S. L.: Protein
988 carbamylation links inflammation, smoking, uremia and atherogenesis, *Nature*
989 *medicine*, 13, 1176-1184, 10.1038/nm1637, 2007.

990 Wang, Z., Yuan, B., Ye, C., Roberts, J., Wisthaler, A., Lin, Y., Li, T., Wu, C., Peng, Y.,
991 Wang, C., Wang, S., Yang, S., Wang, B., Qi, J., Wang, C., Song, W., Hu, W., Wang,
992 X., Xu, W., Ma, N., Kuang, Y., Tao, J., Zhang, Z., Su, H., Cheng, Y., Wang, X., and
993 Shao, M.: High Concentrations of Atmospheric Isocyanic Acid (HNCO) Produced
994 from Secondary Sources in China, *Environmental Science & Technology*, 54, 11818-
995 11826, 10.1021/acs.est.0c02843, 2020.

996 Wentzell, J. J., Liggio, J., Li, S. M., Vlasenko, A., Staebler, R., Lu, G., Poitras, M. J.,
997 Chan, T., and Brook, J. R.: Measurements of gas phase acids in diesel exhaust: a
998 relevant source of HNCO?, *Environmental Science & Technology*, 47, 7663-7671,
999 10.1021/es401127j, 2013.

1000 Woodward-Massey, R., Taha, Y. M., Moussa, S. G., and Osthoff, H. D.: Comparison of
1001 negative-ion proton-transfer with iodide ion chemical ionization mass spectrometry
1002 for quantification of isocyanic acid in ambient air, *Atmospheric Environment*, 98,
1003 693-703, 10.1016/j.atmosenv.2014.09.014, 2014.

1004 Wren, S. N., Liggio, J., Han, Y., Hayden, K., Lu, G., Mihele, C. M., Mittermeier, R. L.,
1005 Stroud, C., Wentzell, J. J. B., and Brook, J. R.: Elucidating real-world vehicle
1006 emission factors from mobile measurements over a large metropolitan region: a focus
1007 on isocyanic acid, hydrogen cyanide, and black carbon, *Atmospheric Chemistry and*
1008 *Physics*, 18, 16979-17001, 10.5194/acp-18-16979-2018, 2018.

1009 Wu, C., Wang, C., Wang, S., Wang, W., Yuan, B., Qi, J., Wang, B., Wang, H., Wang, C.,
1010 Song, W., Wang, X., Hu, W., Lou, S., Ye, C., Peng, Y., Wang, Z., Huangfu, Y., Xie,
1011 Y., Zhu, M., Zheng, J., Wang, X., Jiang, B., Zhang, Z., and Shao, M.: Measurement
1012 report: Important contributions of oxygenated compounds to emissions and
1013 chemistry of volatile organic compounds in urban air, *Atmos. Chem. Phys.*, 20,
1014 14769-14785, <https://doi.org/10.5194/acp-20-14769-2020>, 2020.

1015 Yan, Y., Wang, S., Zhu, J., Guo, Y., Tang, G., Liu, B., An, X., Wang, Y., and Zhou, B.:
1016 Vertically increased NO₃ radical in the nocturnal boundary layer, *Science of The*
1017 *Total Environment*, 763, 142969, <https://doi.org/10.1016/j.scitotenv.2020.142969>,
1018 2021.

1019 Yáñez-Serrano, A. M., Nölscher, A. C., Bourtsoukidis, E., Gomes Alves, E., Ganzeveld,
1020 L., Bonn, B., Wolff, S., Sa, M., Yamasoe, M., Williams, J., Andreae, M. O., and
1021 Kesselmeier, J.: Monoterpene chemical speciation in a tropical rainforest: variation

1022 with season, height, and time of day at the Amazon Tall Tower Observatory (ATTO),
1023 Atmospheric Chemistry and Physics, 18, 3403-3418, 10.5194/acp-18-3403-2018,
1024 2018.

1025 Yao, L., Wang, M. Y., Wang, X. K., Liu, Y. J., Chen, H. F., Zheng, J., Nie, W., Ding, A.
1026 J., Geng, F. H., Wang, D. F., Chen, J. M., Worsnop, D. R., and Wang, L.: Detection
1027 of atmospheric gaseous amines and amides by a high-resolution time-of-flight
1028 chemical ionization mass spectrometer with protonated ethanol reagent ions,
1029 Atmospheric Chemistry and Physics, 16, 14527-14543, 10.5194/acp-16-14527-2016,
1030 2016.

1031 Yu, S.: Role of organic acids (formic, acetic, pyruvic and oxalic) in the formation of
1032 cloud condensation nuclei (CCN): a review, Atmospheric Research, 53, 185-217,
1033 [https://doi.org/10.1016/S0169-8095\(00\)00037-5](https://doi.org/10.1016/S0169-8095(00)00037-5), 2000.

1034 Yuan, B., Koss, A. R., Warneke, C., Coggon, M., Sekimoto, K., and de Gouw, J. A.:
1035 Proton-Transfer-Reaction Mass Spectrometry: Applications in Atmospheric Sciences,
1036 Chemical reviews, 117, 13187-13229, 10.1021/acs.chemrev.7b00325, 2017.

1037 Yuan, B., Shao, M., de Gouw, J., Parrish, D. D., Lu, S., Wang, M., Zeng, L., Zhang, Q.,
1038 Song, Y., Zhang, J., and Hu, M.: Volatile organic compounds (VOCs) in urban air:
1039 How chemistry affects the interpretation of positive matrix factorization (PMF)
1040 analysis, Journal of Geophysical Research: Atmospheres, 117, n/a-n/a,
1041 10.1029/2012jd018236, 2012.

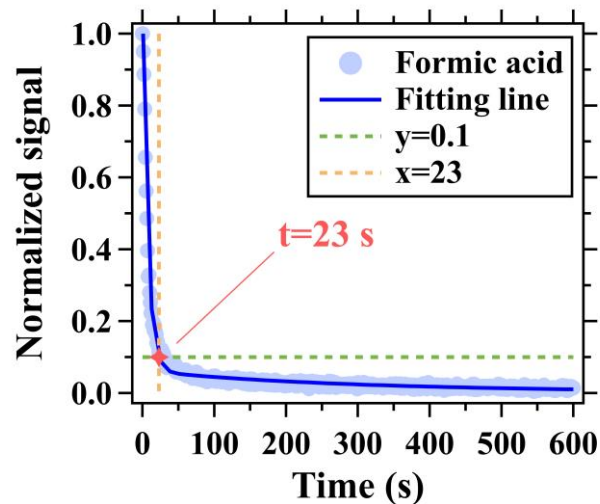
1042 Yuan, B., Veres, P. R., Warneke, C., Roberts, J. M., Gilman, J. B., Koss, A., Edwards,
1043 P. M., Graus, M., Kuster, W. C., Li, S. M., Wild, R. J., Brown, S. S., Dubé, W. P.,
1044 Lerner, B. M., Williams, E. J., Johnson, J. E., Quinn, P. K., Bates, T. S., Lefer, B.,
1045 Hayes, P. L., Jimenez, J. L., Weber, R. J., Zamora, R., Ervens, B., Millet, D. B.,
1046 Rappenglück, B., and de Gouw, J. A.: Investigation of secondary formation of formic
1047 acid: urban environment vs. oil and gas producing region, Atmospheric Chemistry
1048 and Physics, 15, 1975-1993, 10.5194/acp-15-1975-2015, 2015.

1049 Zhao, R., Yin, B., Zhang, N., Wang, J., Geng, C., Wang, X., Han, B., Li, K., Li, P., Yu,
1050 H., Yang, W., and Bai, Z.: Aircraft-based observation of gaseous pollutants in the
1051 lower troposphere over the Beijing-Tianjin-Hebei region, Science of The Total
1052 Environment, 773, 144818, 10.1016/j.scitotenv.2020.144818, 2021.

1053 Zhao, R., Lee, A. K. Y., Wentzell, J. J. B., McDonald, A. M., Toom-Saunty, D., Leaitch,
1054 W. R., Modini, R. L., Corrigan, A. L., Russell, L. M., Noone, K. J., Schroder, J. C.,
1055 Bertram, A. K., Hawkins, L. N., Abbatt, J. P. D., and Liggio, J.: Cloud partitioning
1056 of isocyanic acid (HNCO) and evidence of secondary source of HNCO in ambient
1057 air, Geophysical Research Letters, 41, 6962-6969, 10.1002/2014gl061112, 2014.

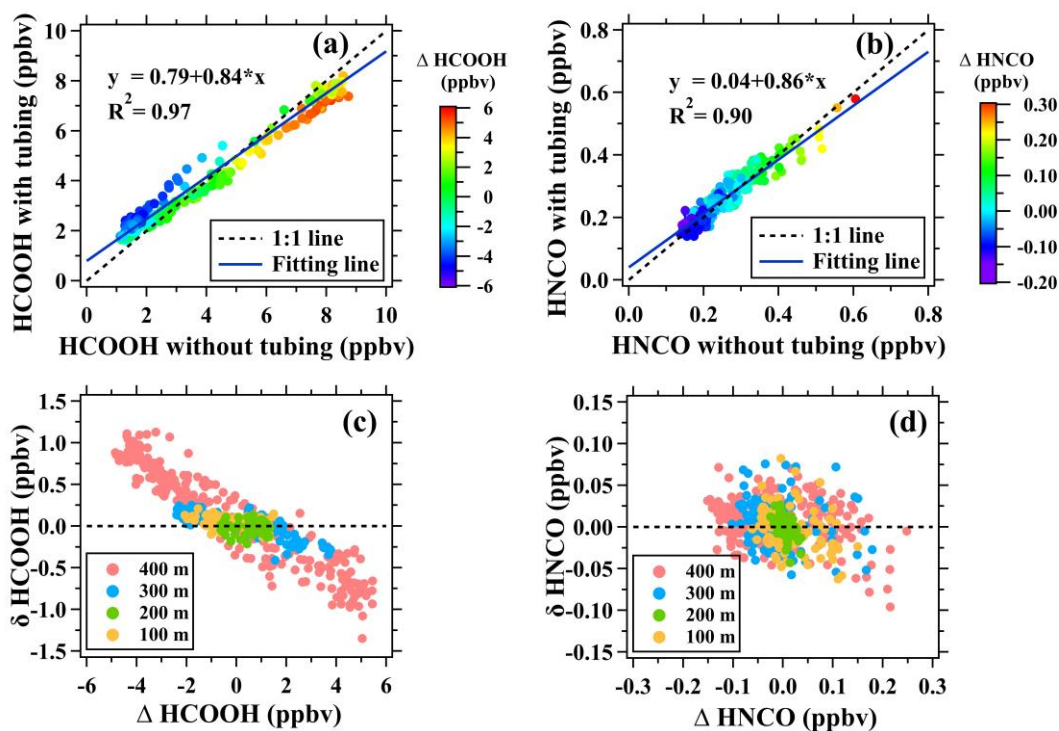
1058 Zhu, B., Han, Y., Wang, C., Huang, X., Xia, S., Niu, Y., Yin, Z., and He, L.:
1059 Understanding primary and secondary sources of ambient oxygenated volatile
1060 organic compounds in Shenzhen utilizing photochemical age-based parameterization
1061 method, Journal of Environmental Sciences (China), 75, 105-114,
1062 10.1016/j.jes.2018.03.008, 2019.

1063



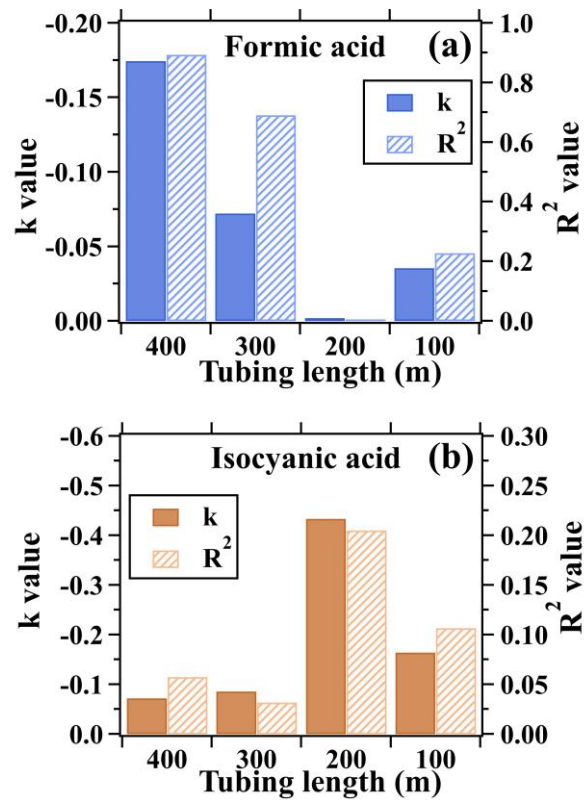
1064

1065 **Figure 1.** Depassivation curves of formic acid signal measured by I⁻ ToF-CIMS for the
1066 400 m long tubing at the flow rate of 13 SLPM. Ion signals were normalized to those
1067 measured at the start time (0 s) of the step-function change.



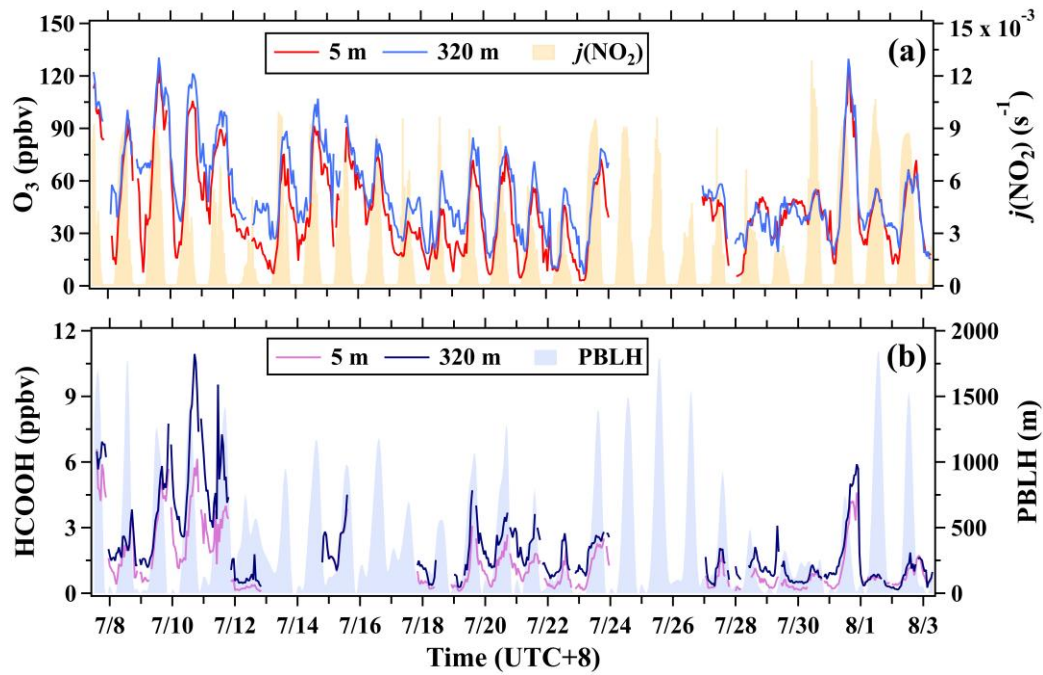
1068

1069 **Figure 2.** Assessment of long tubes in measuring formic and isocyanic acids in ambient
 1070 air. (a-b) Scatterplots of mixing ratios of formic and isocyanic acids measured with the
 1071 400 m long tube versus those measured without the long tube. (c-d) Scatterplots of
 1072 $\Delta[HCOOH]$ versus $\delta[HCOOH]$ and scatterplots of $\Delta[HNCO]$ versus $\delta[HNCO]$ for
 1073 the 100, 200, 300, and 400 m tubes.



1074

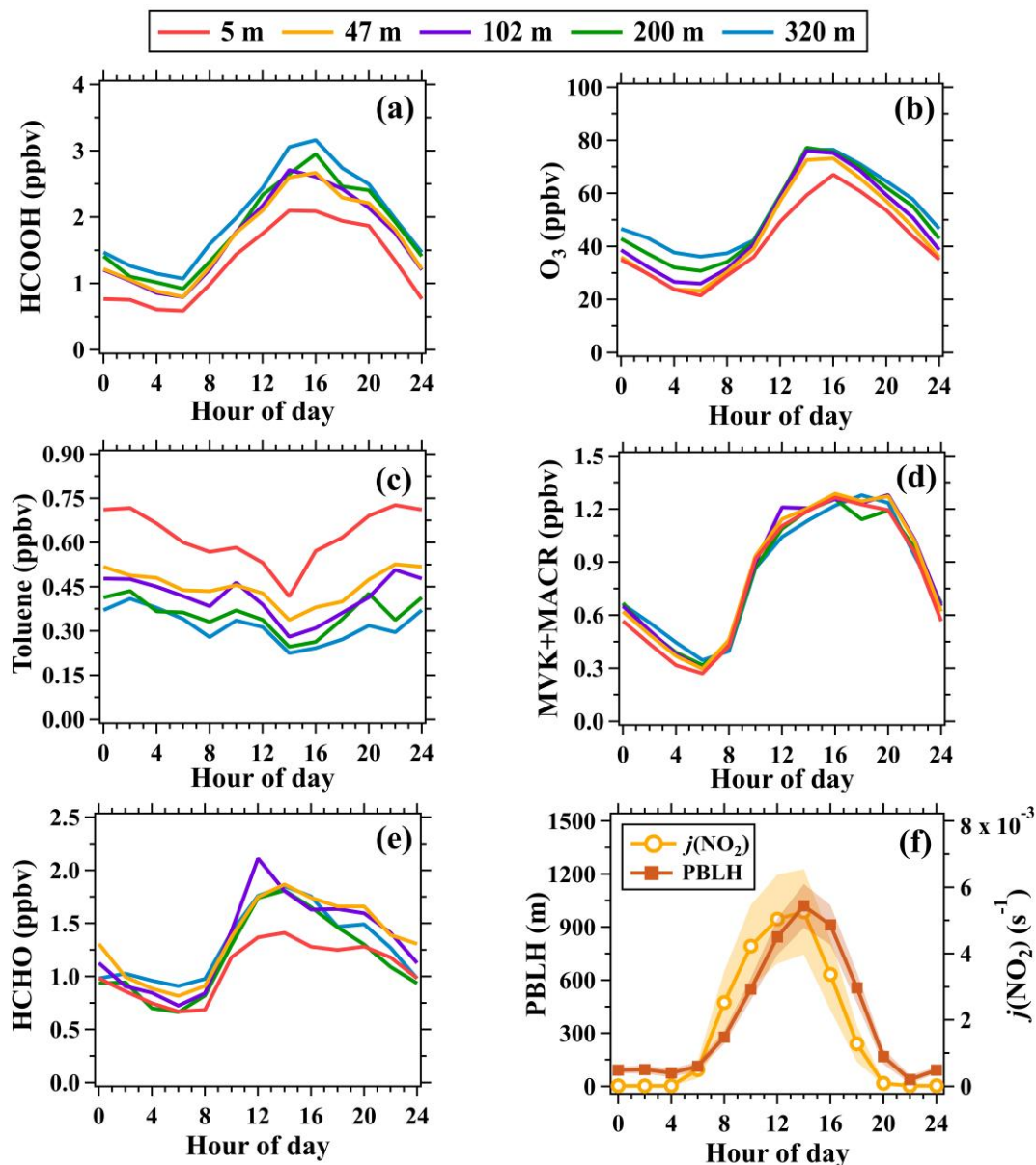
1075 **Figure 3.** Linear fitting parameters (namely k and R^2) for (a) $\Delta[HCOOH]$ versus
 1076 $\delta[HCOOH]$ and (b) $\Delta[HNCO]$ versus $\delta[HNCO]$. The scatterplots are shown in
 1077 Figure 2. k and R^2 are the slope and determination coefficient of the linear fitting lines,
 1078 respectively.



1079

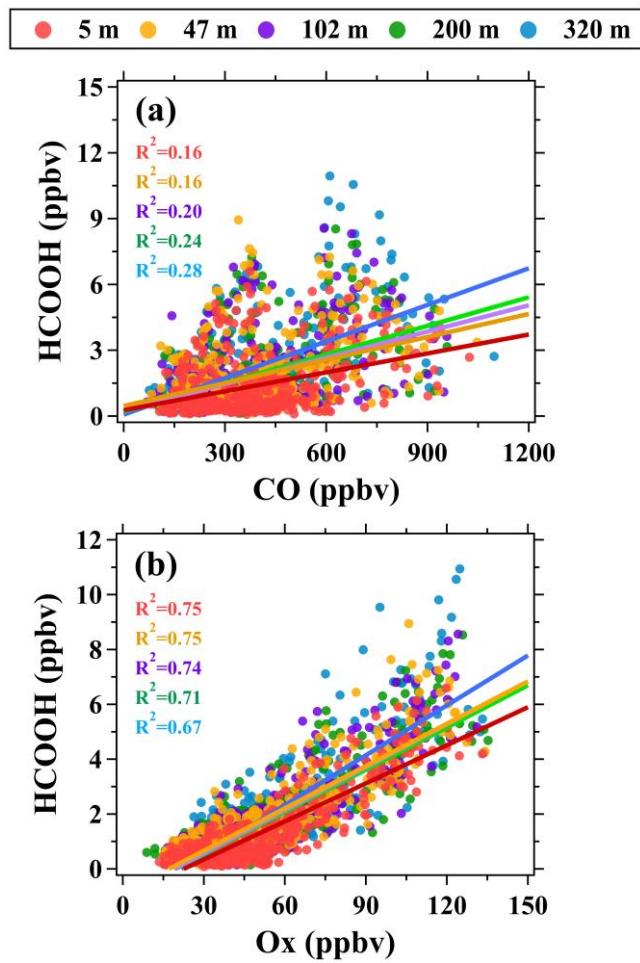
1080 **Figure 4.** Time series of (a) O₃ (5 and 320 m), $j(\text{NO}_2)$, (b) formic acid (5 and 320 m),

1081 and planetary boundary layer height (PBLH) during the campaign.



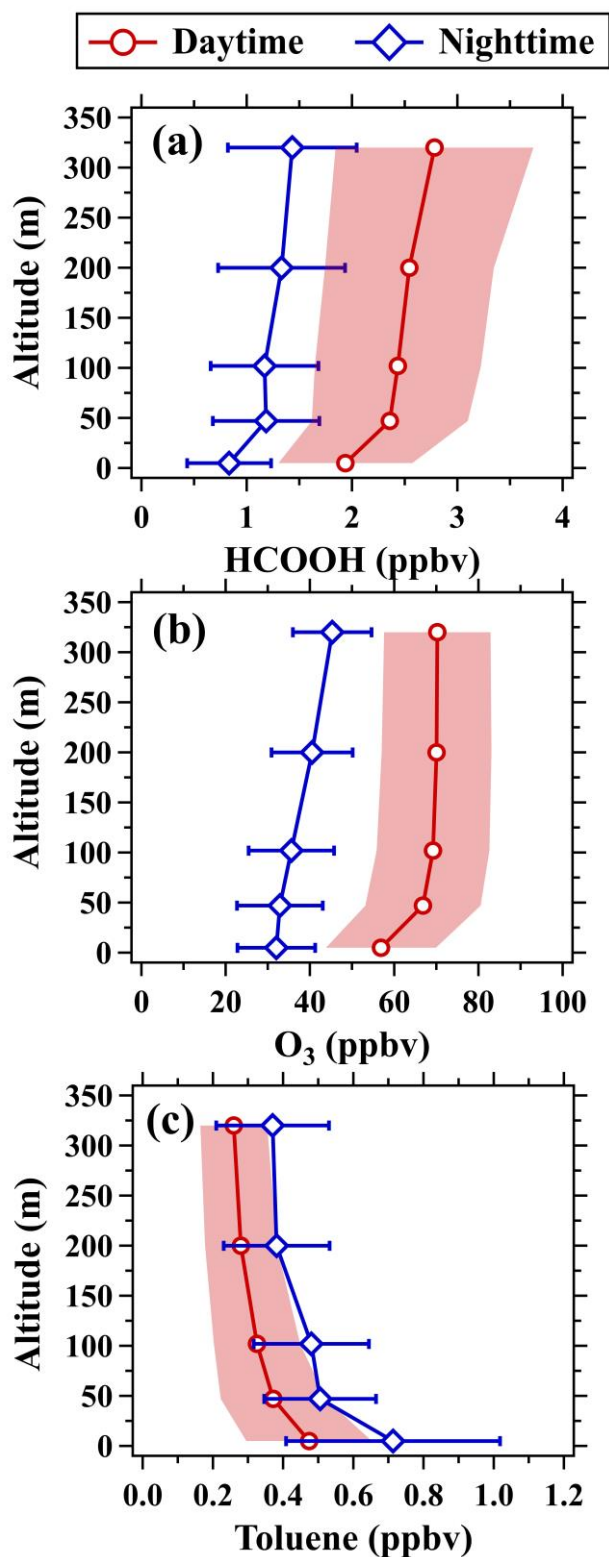
1082

1083 **Figure 5.** Average diurnal variations in mixing ratios of (a) formic acid, (b) O₃, (c)
 1084 toluene, (d) MVK+MACR, (e) formaldehyde at the five inlet heights and (f) PBLH and
 1085 $j(\text{NO}_2)$. The shaded areas in panel (f) are half of the standard deviations. Average diurnal
 1086 variations in mixing ratios of (a) formic acid, (b) O₃, (c) toluene, (d) MVK+MACR and
 1087 (e) formaldehyde at 5, 47, 102, 200, and 320 m. (f) Average diurnal variations in mixing
 1088 ratios (5 m) and CICs of formic acid during the field campaign; The shaded areas in
 1089 panel (e) are half of the standard deviations.



1090

1091 **Figure 6.** Scatter plots of (a) formic acid versus CO and (b) formic acid versus Ox at
 1092 different altitudes during the campaign.

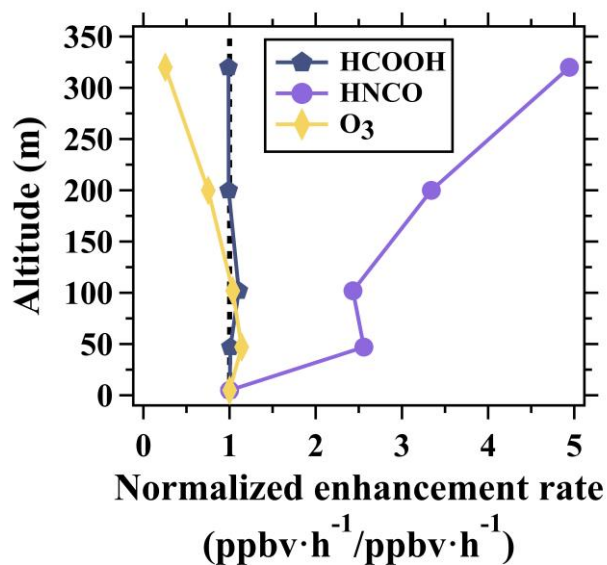


1093

1094 **Figure 7.** Vertical profiles of (a) formic acid, (b) O₃, and (c) toluene in daytime (11:00-

1095 16:00 LT) and nighttime (22:00-5:00 LT). The shaded areas and error bars are half of

1096 the standard deviations.



1097

1098 **Figure 8.** Normalized vertical profiles of the enhancement rate of ozone, formic acid,

1099 and isocyanic acid between 6:00-10:00 LT averaged over the whole campaign.

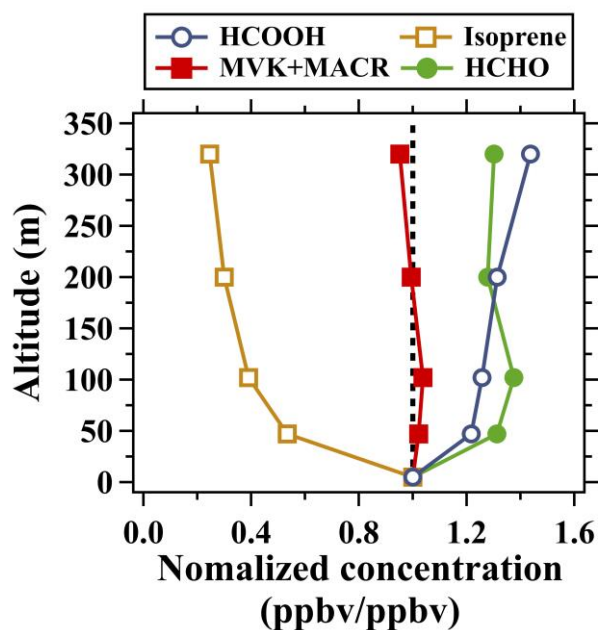
1100 Enhancement rate of the species at different altitudes were normalized to those at 5 m.

1101 The dotted line indicates the normalized enhancement rate of 1.~~Normalized vertical~~

1102 ~~profiles of the growth rates of ozone, formic acid, and isocyanic acid between 6:00-~~

1103 ~~10:00 LT averaged over the whole campaign. Growth rates of the species at different~~

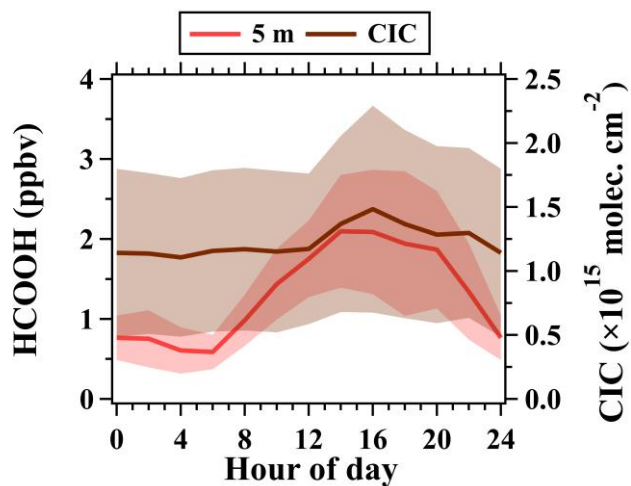
1104 ~~altitudes were normalized to those at 5 m.~~



1105

1106 **Figure 9.** Normalized vertical profiles of formic acid, isoprene, formaldehyde, MVK
 1107 and MACR in daytime (11:00-16:00 LT) averaged over the whole campaign. Mixing
 1108 ratios of the species at different altitudes were normalized to those at 5 m. The dotted
 1109 line indicates the normalized concentration of 1.~~Normalized vertical profiles of formic~~
 1110 ~~acid, isoprene, formaldehyde, MVK and MACR in daytime (11:00-16:00 LT) averaged~~
 1111 ~~over the whole campaign. Mixing ratios of the species at different altitudes were~~
 1112 ~~normalized to those at 5 m.~~

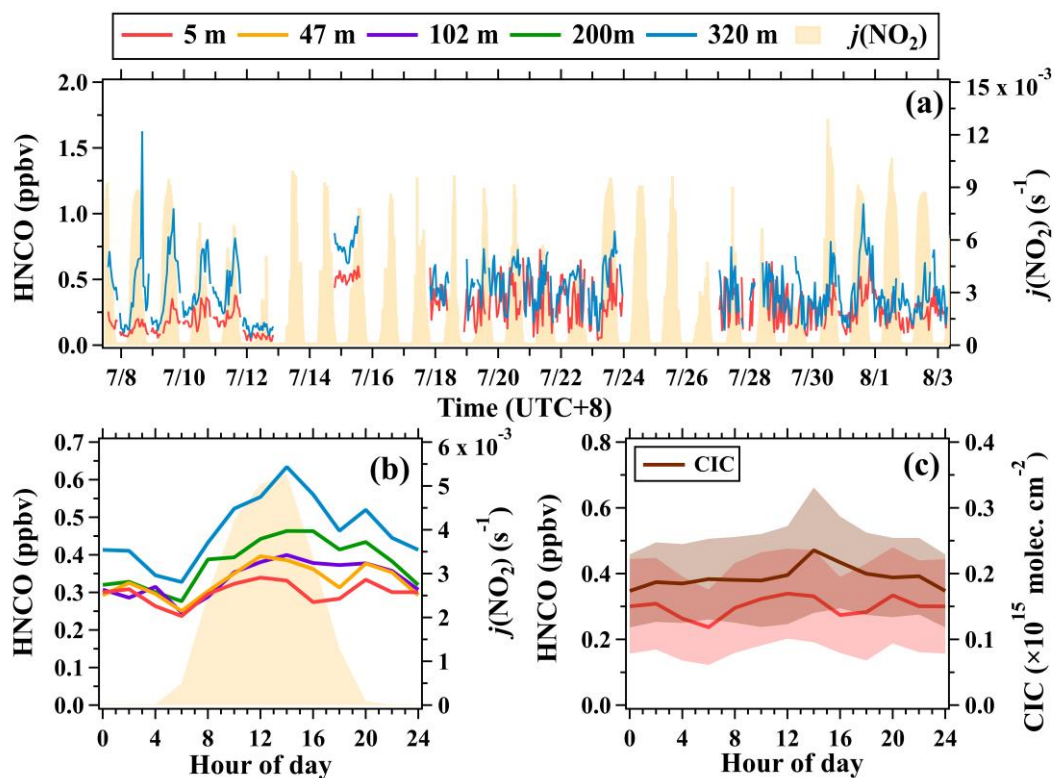
1113



1114

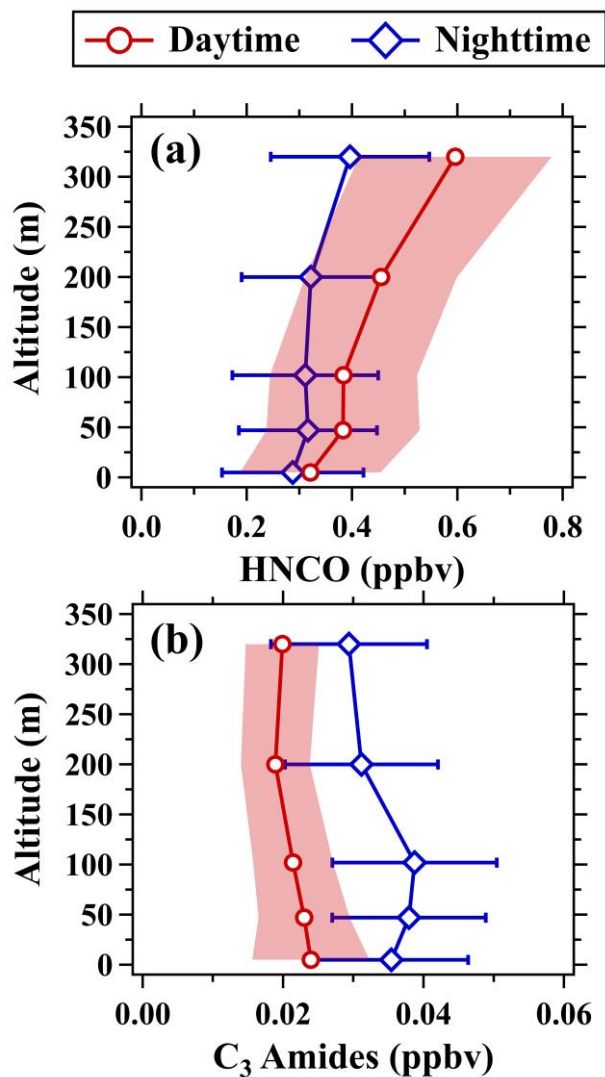
1115 [Figure 10. Average diurnal variations in mixing ratios \(5 m\) and CICs of formic acid](#)

1116 [during the field campaign; The shaded areas are half of the standard deviations.](#)



1117

1118 **Figure 10.11.** (a) Time series of isocyanic acid (5 and 320 m) and $j(\text{NO}_2)$. (b) Average
 1119 diurnal variations in isocyanic acid at 5, 47, 102, 200, and 320 m. (c) Average diurnal
 1120 variations in mixing ratios (5 m) and CICs of isocyanic acid during the campaign; The
 1121 shaded areas in panel (c) are half of the standard deviations.



1122

1123

Figure 112. Vertical profiles of (a) isocyanic acid and (b) C₃ amides in daytime

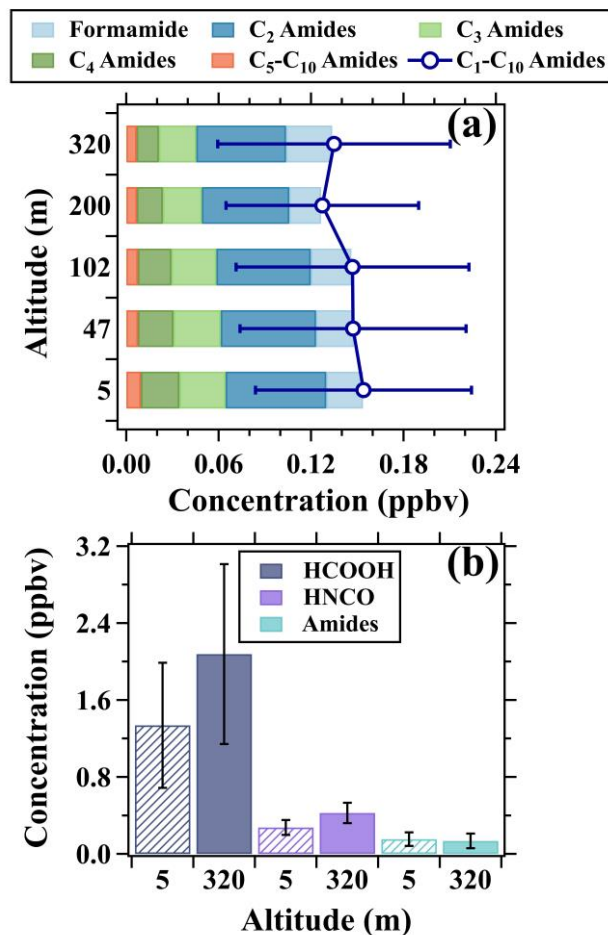
1124

(11:00-16:00 LT) and nighttime (22:00-5:00 LT). The shaded areas and error bars are

1125

half of the standard deviations.

1126



1127

1128 **Figure 12.13.** (a) Vertical variations in composition and concentrations of amides. (b)
 1129 Concentration comparison of formic acid, isocyanic acid, and amides between 5 and
 1130 320 m. The data in both (a) and (b) was the average results of the whole campaign. The
 1131 patterns of the bars are used to distinguish the average concentration of the species at
 1132 the two heights. (a) Vertical variations in composition and concentrations of amides. (b)
 1133 Concentration comparison of formic acid, isocyanic acid, and amides between 5 and
 1134 320 m. The data in both (a) and (b) was the average results of the whole campaign.